CHARACTERISTICS OF VORTEX IN THE SCOUR HOLE

by

KAILASH GUPTA

DEPARTMENT OF CIVIL ENGINEERING

INDIAN INSTITUTE OF TECHNOLOGY, KANPUR

JANUARY, 1986

CHARACTERISTICS OF VORTEX IN THE SCOUR HOLE

A Thesis Submitted
in Partial Fulfilment of the Requirements
for the Degree of

MASTER OF TECHNOLOGY

by

KAILASH GUPTA

to the

DEPARTMENT OF CIVIL ENGINEERING

INDIAN INSTITUTE OF TECHNOLOGY KANPUR

JANUARY, 1986

DEDICATED

TO

MY PARENTS

6/1/86

CERTIFICATE

The thesis entitled 'Characteristics of Vortex in the Scour Hole' , by Kailash Gupta (Roll No.8410317) is hereby approved as a creditable report on research carried out and present in a manner which warrants its acceptance as a prerequisite for the degree of Master of Technology. The work has been carried out under my supervision and has not been submitted elsewhere for a degree.

January, 1986

(Dr. T. GANGADHARAIAH)
Professor
Department of Civil Engineering
Indian Institute of Technology, Kanpur

ACKNOWLEDGEMENTS

I lack words to express my gratitude to Dr. T. Gangadhariah for his constant help, guidance and encouragement during the work.

I take this opportunity to thank Dr. V. Lakshminarayana, Dr. K. Subramanya, Dr. S. Surya Rao and Dr. S. Ramaseshan of the Department of Civil Engineering for useful courses I received from them during the first two semesters of the degree programme.

The cooperation received from the staff of the Hydraulics and Water Resources Laboratory of the Department of Civil Engineering, is gratefully acknowledged.

Thanks are due to my friend Ms. Rajani Gupta for her constant encourgement and inspiration.

Thanks are also due to Mr. Gautam Ray for his kind help and suggestions in the thesis report writing , Dr. Sullery of the Department of Aero-dynamics for his kind suggestion to use the vorticity probe, Mr. Muddappa of Departmen of Aero-dynamics for fabricating the vorticity probe.

I am obliged to Prof. Ali Mul Qadar of A.M.U. for supplying his experimental data for the analysis.

And finally, thanks to Mr. G.S. Trivedi for an excellent job of typing.

KAILASH GUPTA

CONTENTS

LIST OF FIGURES

NOTATIONS

D	-	Diameter of cylinder
Fr	-	Froud number $\bar{V}/\sqrt{gh_o}$
I	-	Hydraulic gradient
P_e	-	Perimeter of elliptical vortex
R_{eD}	-	Pier Reynolds number
U	-	Velocity at a point
U_o	-	Free stream velocity or maximum velocity
$\bar{U}$	-	Average velocity
$\bar{U}_c$	-	Critical velocity
V_*	-	Shear velocity $=\sqrt{\tau_o/\rho}$
V_{*c} = $V_{*c(50)}$	-	Threshold velocity, as per shield's criterian for d_{50}
$V_{*c(90)}$	-	Threshold velocity as per shield's criterian for d_{90}
V_θ	-	Rotational velocity
$V_{\theta o}$	-	Maximum rotation velocity
a	-	Major axis of elliptical vortex
b	-	Minor axis of elliptical vortex
d	-	Mean of sediment size
d_{50}	-	Size of sediment such that 50 percent particles are finer than this size
d_{90}	-	Size of sediment such that 90 percent particles are finer than this size
h_o	-	Depth of flow
h_s	-	Depth of scour
h_{sm}	-	Maximum depth of scour

δ	-	Boundary layer thickness
ρ	-	Mass density of fluid
ν	-	Kinematic viscosity
σ_d	-	Standard deviation of sediment size distribution
Γ	-	Circulation or strength of horse-shoe vortices
Γ_o	-	Initial strength of vortex
Γ_e	-	Strength of vortex at equilibrium condition of scour

ABSTRACT

In the present investigation flow around a circular cylinder mounted on a mobile bed was studied. Two different types of sand were used to study the probable effect of grain size. Attempts were made to analyse the basic mechanism of scour, that is, horse-shoe vortex, by measuring its vorticity mechanically with the help of a probe. In addition to this data available in literature are analysed to get an insight in the scour mechanism.

From the analysis of data available in literature it is concluded that the horse-shoe vortex gradually assumes an elliptical shape as the scour hole develops and the resulting in forced type of vortex. Strength and size of initial vortex are found to be functions of Pier Reynolds number. From the present vorticity measurements it is found that vorticity decays very fast with scour development. Based on available data and results of the present experiments a vortex model is proposed for prediction of scour depth.

CHAPTER 1

INTRODUCTION AND LITERATURE SURVEY

1.1 Introduction:

It is well known that an obstruction such as a bridge pier placed against the direction of flow over a mobile bed leads to the scouring of sediment around it. Knowledge of the magnitude of this scour is very important in safe and economic design of foundations of bridge piers. Till date enough data have been collected in laboratories as well as in the field with a view to adequately predict the maximum depth of scour. However, relatively little is known about the mechanism of scour, because of the processes involved of water and sediment movement are complicated. Major contributors to the understanding of the mechanics of scour include investigators like Tison (4), Keuthner (4), Posey (9), Laursen and Toch (6), Roper at al. (11), Baker (2), Melville and Raudkivi (8), and Qadar (10).

1.1.1 Description of flow field around a pier:

The scouring process around bridge piers is due to horse-shoe vortex systems. The vortex filaments transverse to the flow in a two dimensional undisturbed velocity field, are concentrated by the presence of a blunt-nosed pier to form the horse-shoe vortex system (a blunt-nosed pier is one

which induces a sufficiently large pressure gradient to initiate the concentration of vortex filaments described above. All other piers are referred to as sharp-nosed). This concentration of vortex filaments is due to the pressure field induced by the pier. Figs. (1.1) and (1.2) have been given to aid the understanding of the horse-shoe vortex system. The system is not steady for all flow conditions studied. Schwind (1962) noted that for some Reynolds numbers the horse-shoe vortex is shed periodically. The strength of the horse-shoe vortex is determined largely by the geometry of the pier. To some extent the condition of bed also affects the strength.

Melville (1975) found that a strong vertically downward flow developed ahead of the cylinder as the scour hole enlarged. The size and the circulation of the horse-shoe vortex increased rapidly and the velocity near the bottom of the hole decreased as the scour hole enlarged.

1.1.2 Scour process:

The dominant feature of scour process around a blunt-nosed pier is the horse-shoe vortex system. If the strength of this system is strong enough to overcome the particles resistance to motion, scour will be initiated. Sediment particles will be disloged free upstream of the pier and carried out of the scour hole either by the horse-shoe vortex

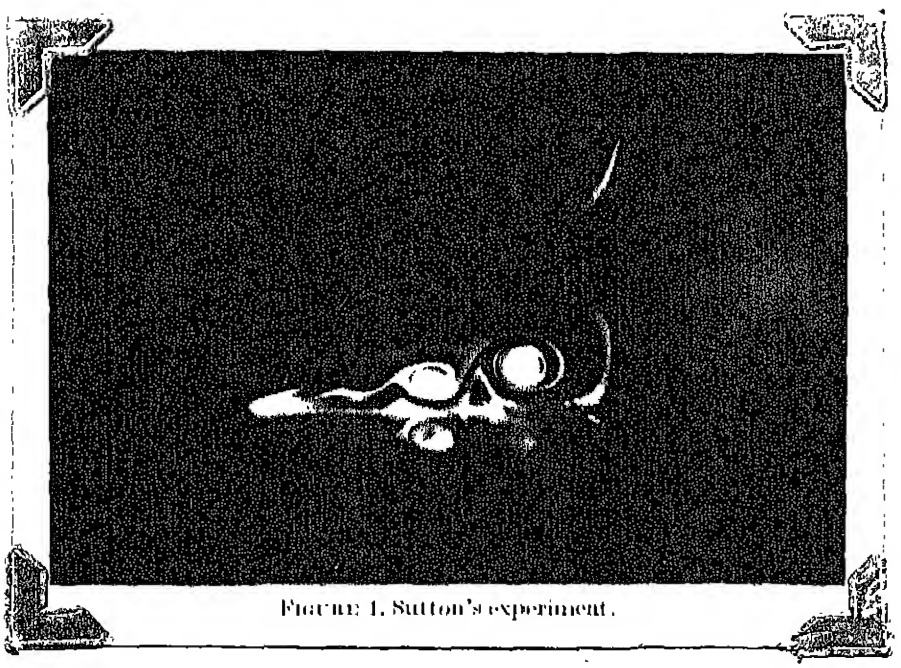

FIGURE 1. Sutton's experiment.

Fig. 1.1 : HORSE SHOE VORTEX SYSTEM

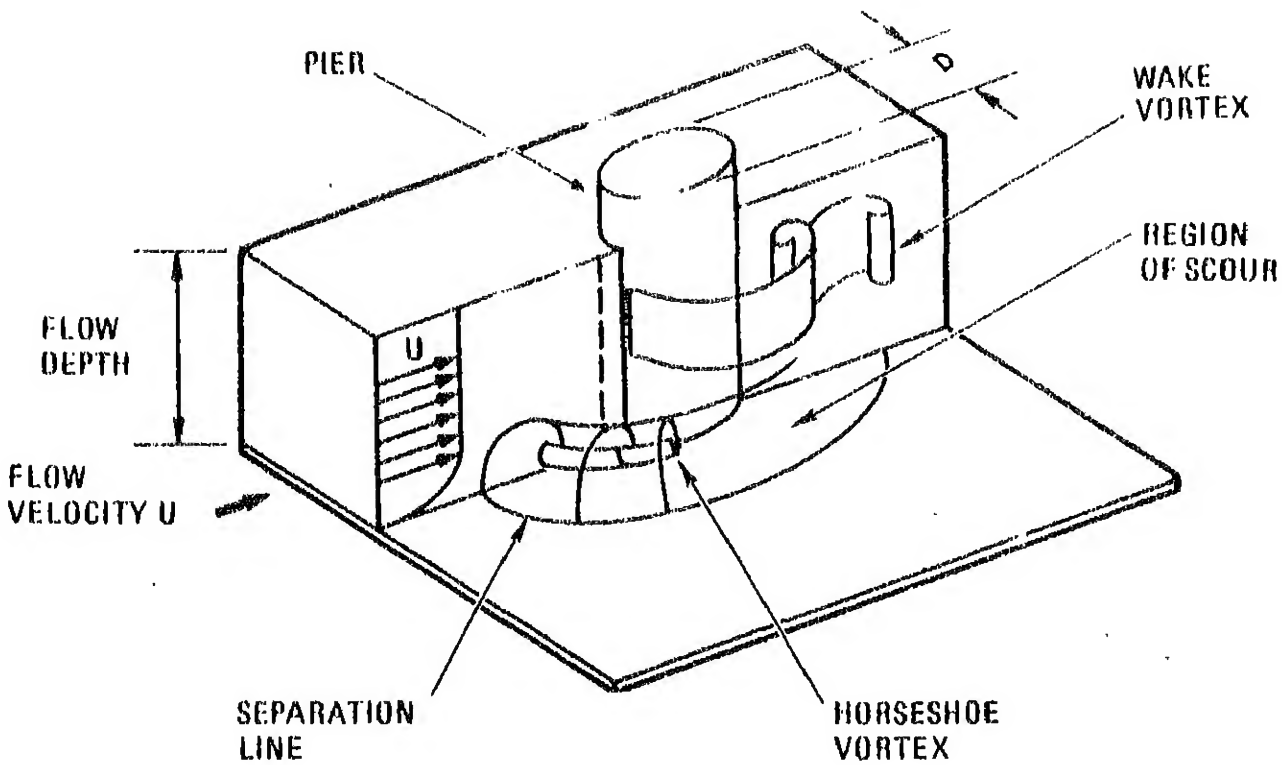

Fig. 1.2 Scour around a pier

system and/or by the wake vortex system on the downstream side of the pier.

As a scour hole forms beneath the vortex system, the vortex system sinks into the scour hole. Melville and Raudkivi (8) point out that the vortex strength increases initially as the vortex system sinks in the scour hole, because additional fluid attains downward motion. However Baker (2) disagrees with Melville's hypothesis of increase in strength of vortex.

Both Melville and Raudkivi, and Baker observed the increase in size of the vortex as it sinks in the scour hole. As the depth of scour increases, the rotational velocity of the vortex system decreases, causing decrease in the shear stress beneath the vortex system. This process continues till the equilibrium condition is reached. The equilibrium condition indicates the state when the rotational velocity of vortex can no longer dislodge the surface grains at the bed. In the case of live upstream bed, the equilibrium condition oscillates with the movements of upstream bed forms into the scour hole.

1.1.3 Analyses of scouring parameters:

Limiting our attention to the case of the isolated bridge pier which has been modelled as a circular cylinder, there are many parameters which may influence the scouring

phenomenon:

Variables characterizing the fluid:

- g acceleration due to gravity,
- ρ density of fluid, and
- ν kinematic viscosity of fluid.

Variables characterizing the bed material:

- ρ_s density of the sediment,
- size distribution,
- grain form, and
- cohesion of material.

Variables characterizing the flow:

- h_o depth of approach flow,
- $\bar{U}$ mean velocity of undisturbed flow, and
- k the roughness of the approach flow.

Variables characterizing the bridge pier:

- its shape,
- its dimensions, (diameter, D in case of circular pier),
- its surface condition, and
- any protection systems.

Assuming that (1) the sediment is non-cohesive and has a uniform size, d_{50} ; (2) channel is sufficiently wide and with a flat bed (without dunes or ripples) ; (3) pier is

cylindrical, circular and perfectly smooth, the scouring depth h_s depends upon eight parameters:

$$h_s = f_1(\rho, \nu, g, d_{50}\rho_s, h_o, \bar{U}, D)$$

These parameters may be replaced by the following ones:

$$h_s = f_2(\rho, \nu, g, d_{50}, h_o, \bar{U}, D)$$

with $\Delta = (\rho_s - \rho) / \rho$, the relative submerged density and $\bar{U}_c = (g\, h_o\, I)^{1/2}$, where I is the hydraulic gradient.

The theorem of Vaschy-Buckingham allows us to write:

$$\frac{h_s}{D} = f_3\left(\frac{\bar{U} d_{50}}{\nu}, \frac{\bar{U}^2}{\Delta g\, d_{50}}, \Delta, \frac{h_o}{D}, \frac{d_{50}}{D}\right) \ldots (1)$$

Eqn. (1) can be considerably simplified by the following considerations:

- The influence of the deformation of the free surface on the flow field is negligible if the Froude number of the flow is sufficiently low.

- There is an emperical relation for initiation of motion, relating

$$\frac{\bar{U}_c d_{50}}{\nu} \quad \text{and} \quad \frac{\bar{U}_c^2}{\Delta g\, d_{50}}$$

- The term Δ is constant by considering only natural sediments (pebbles, gravel or sand, $\Delta \simeq 1.65$). Under these assumptions Equation (1) may be simplified to:

$$\frac{h_s}{D} = f\left(\frac{\bar{U}}{\bar{U}_c}, \frac{h_o}{D}, \frac{d_{50}}{D}\right) \text{ or } \frac{h_{sm}}{D} = f\left(\frac{h_o}{D}, \frac{d_{50}}{D}\right)$$

This means that the scour depth h_s will depend mainly on the ratio of mean velocity to mean critical velocity and the relative values of grain size, flow depth and pier diameter.

1.2 Literature Survey:

1.2.1 Description of model data:

Some of the most important literature on the subject are summerised below:

Chabert and Engeldinger (1956) (4) studied the influence of flow velocity and showed that two regimes should be distinguished for velocities at or below the threshold velocity of movement of the bed material , scour depth approaches a limit asymptotically (see Fig. 1.3) whereas for a larger velocity scour depth fluctuates due to the periodic dumping of material in the scour hole by moving dunes (Fig. 1.4). Maximum scour depth was obtained at velocities near the threshold velocity, whereas scour started at about half the threshold velocity (Fig. 1.5).

The influence of grain size, pier diameter and water depth can be seen from Fig. 1.6, which shows a small influence of grain size, a negligible influence of water depth for water

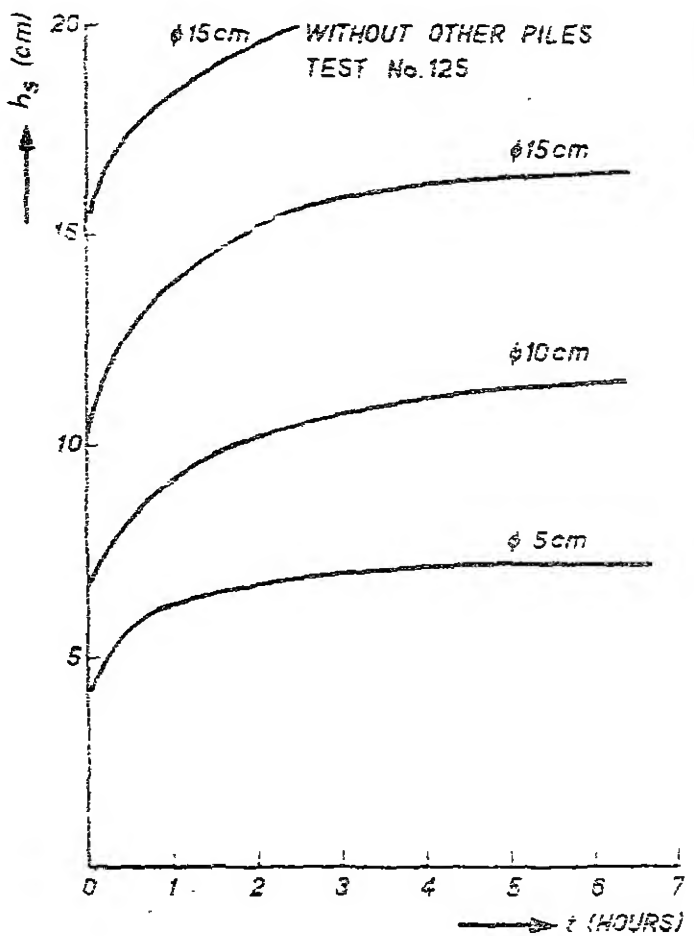

TEST No. 113 $d_{50} = 3$ mm
$h_o = 20$ cm
$\bar{U} = 52$ cm/s

Fig. 1.3 Scour as a function of time $\bar{U} < \bar{U}_c$. (ref. 4)

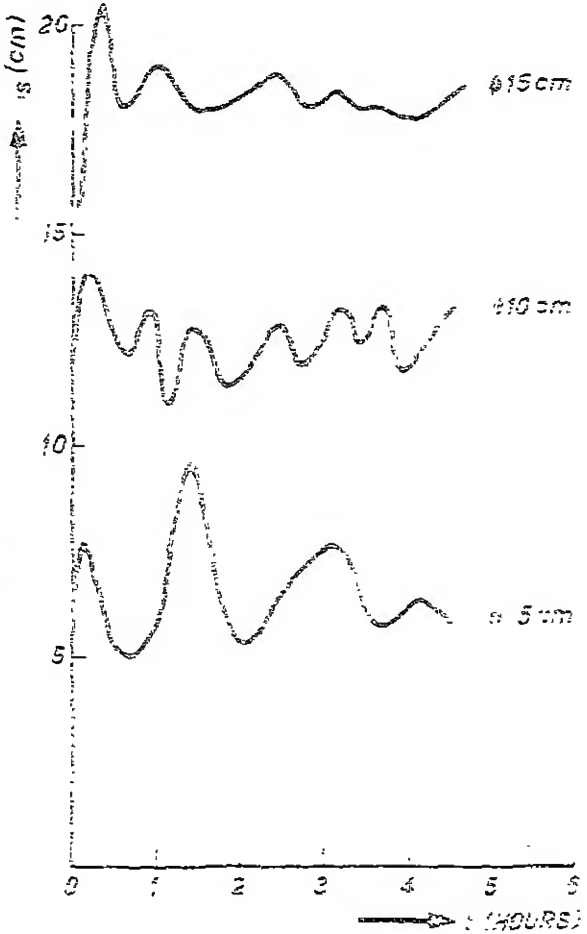

TEST No. 112 $d_{50} = 3$ mm
$h_o = 20$ cm
$\bar{U} = 52$ cm/s

Fig. 1.4 Scour as a function of time $\bar{U} > \bar{U}_c$. (ref. 4)

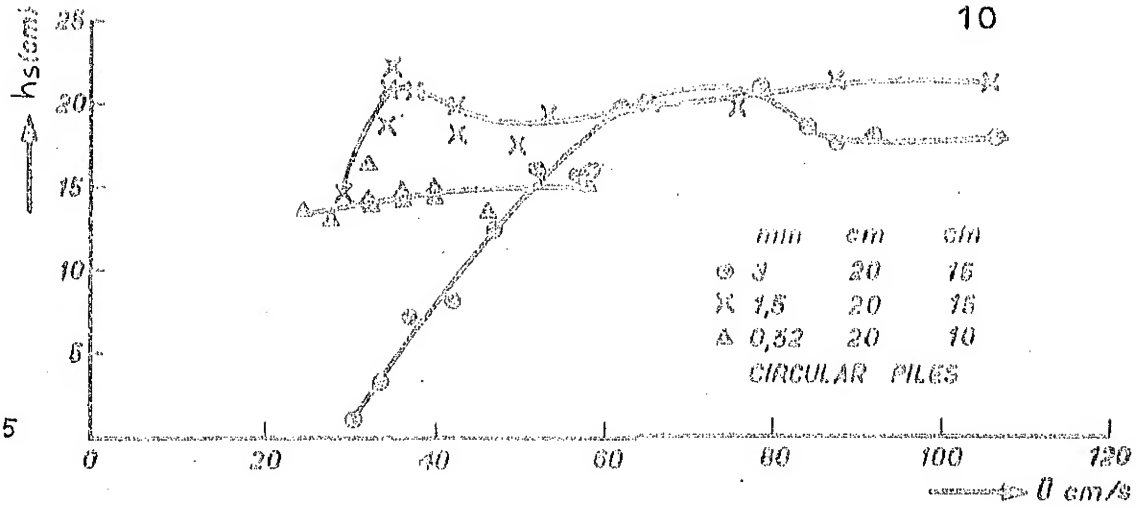

Fig. 1.5

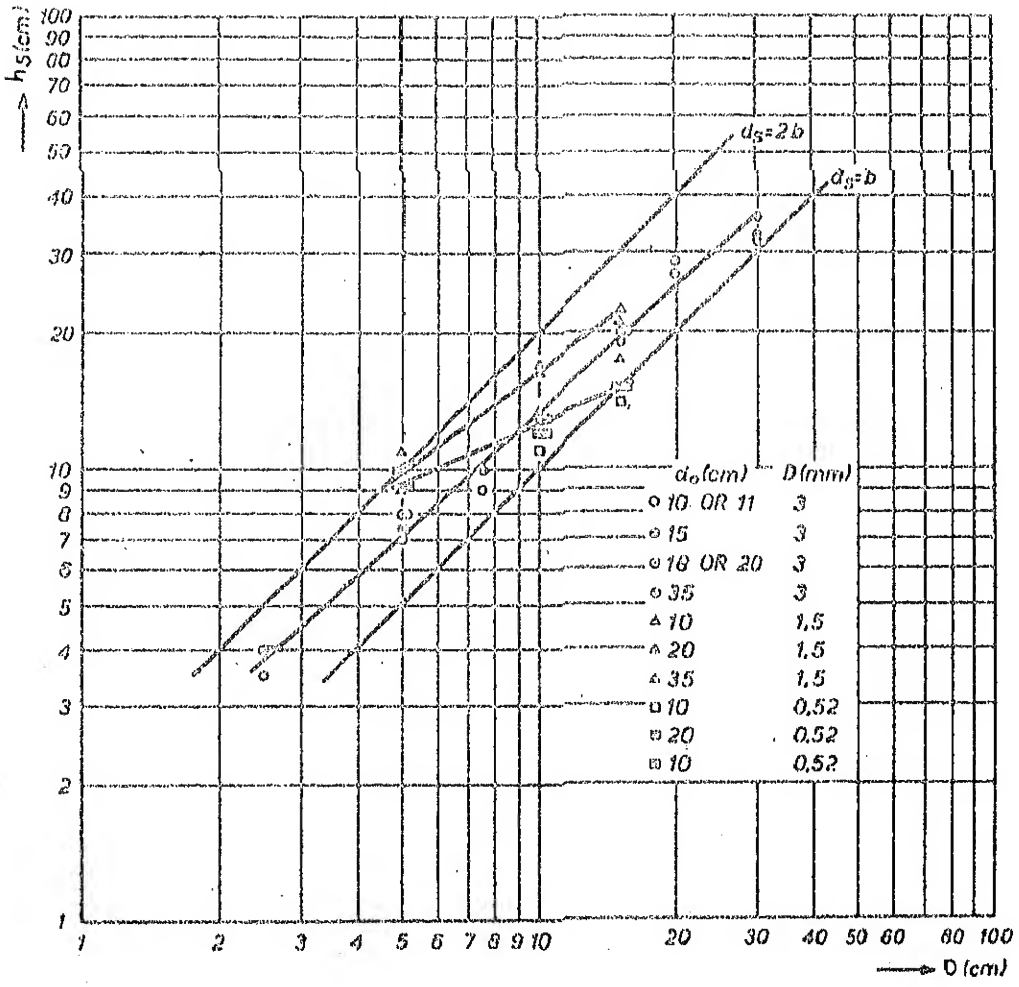

Fig. 1.6

Fig. 1.5 : Scour Depth Variation with Threshold Velocity (ref.4)

Fig. 1.6: Influence of grain size, pier diameter and water depth on scour depth. (ref.4)

depth/pier diameter ratios larger than one, and an increase of scour with D^{α} in which $\alpha \leq 1$ and D is the diameter of the pier.

Laursen and Toch (1956,1953)(16)studied the influence of water depth, mean flow velocity and sediment size with a dumb-bell pier under an angle of attack of 30^{o}. The results are given in Fig. 1.7, from which it was concluded that there was no systematic influence of grain size and velocity in the range studied. There is an influence of water depth as is clear from the Fig. 1.7.

Shen, Schneider, Karaki (1966a,b, 1969) (4), Roper, Schneider, Shen (1967) (4), Shen (1971) (4) . From an analysis of the flow field and the horse-shoe vortex system near a circular pier it was concluded that the circulation of the vortex is proportional to $\bar{U}$. a (a = b/2). The influence of grain size was considered to be neglegible for $d < 0.5$ mm. Roughening the upstream face of the pier to decrease the vertical velocities or the strength of the vortex had no effect.

Roper et al. (1967) (11) proposed a vortex model based on the assumption of potential flow approaching the cylinder using a control volume approach. They related the scour depth to Reynolds number $\bar{U}\ D/\nu$, where $\bar{U}$ is the average velocity of the approaching flow and ν is the kinematic viscosity of the fluid.

Fig. 1.7

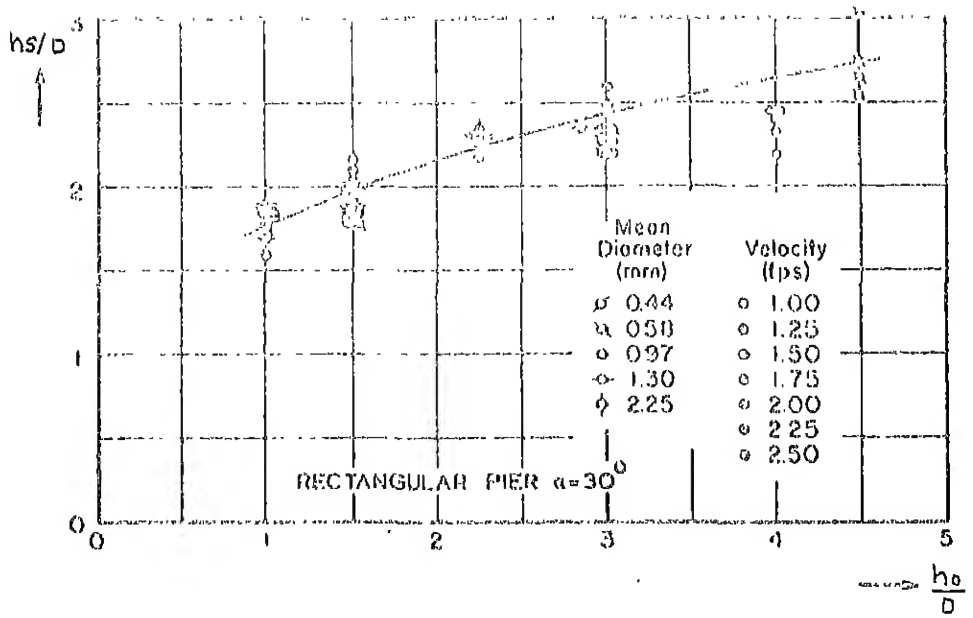

Fig. 1.7 : Scour as a function of water depth, mean flow velocity and sediment size. (Ref. 4)

Baker, 1981 (2) proposed a vortex model based on the assumption that the circulation of vortex remains same throughout the scouring process, only the size of the vortex increases and correspondingly the rotational velocity of the vortex decreases. Based on these considerations, he found that the non-dimensional scour depth varies with Froude's parameter $\bar{U}/\sqrt{g\ D}$.

Baker's model provides a basis for semi-empirical correlation of the variation of the equilibrium scour depth upstream of a circular cylinder in a bed of sand, with the various flow parameters. For clear water scour

$$\frac{h_{se}}{D} = (a_1 N - a_2) \tanh \left(a_3 \frac{h}{D} \right)$$

where $a_1, a_2, a_3 = fn\ (h/d, c)$

$$G = \left(\frac{\rho_s}{\rho} - 1 \right) g\ d^3/\nu^2$$

$$N = \bar{U} / \left[\left(\frac{\rho_s}{\rho} - 1 \right) g\ d \right]^{1/2}$$

Qadar(11) measured the rotational velocity and size of the vortex before scour and related these to the approaching flow's average velocity and obstruction width respectively.

Gupta (5) observed that the first separation point on the plate upstream of the cylinder occurs around $r/D \simeq 1.5$ at $\vartheta = 0^{o}$. He postulated the presence of three major vortices on the plate at the front of cylinder. A method of

computation of strength of horse-shoe vortex from the pressure distribution on the plate was developed.

Muzzammil (9) found that the diameter of the horse-shoe vortex varies from 0.2 D to 0.6 D. He related the maximum scour depth with the initial strength of the horse-shoe vorticies and the upstream vorticity parameter. The pressure distribution on the surface of cylinder before and after scour was studied, and it was found that the pressure remains the same above the bed level and decreases inside the scour hole indicating the recovery of pressure. He observed that the d_{50} of the sediment in the scour hole corresponds to d_{90} of the original bed sediment, indicating the armour effect in the scour hole.

1.2.2 Description of field data:

Inglis, 1949 (4) compared the total scour depth (sum of general scoured depth, scour due to contraction and local scour due to the piers) with the Lacey regime depth:

$$h_{s(Lacey)} = 0.473\ (Q/f)^{1/3} \quad (\text{in M.K.S.})$$

in which f = silt factor = $1.76\sqrt{d_{50}}$, d_{50} = median grain size in mm. The average value was 2.09 with a r.m.s. value of 12.9 percent. For design purposes generally a value of 2.0 is used, therefore:

$$\text{Total scour depth} = 0.95\ (Q/f)^{1/2}.$$

Arunachalam, 1965 (4) reanalysed the data and found that the correlation could be improved by leaving f out of correlation. The result was:

Total scour depth = (2.09) 0.473 $Q^{1/3}$ ≃ 0.95 $Q^{1/3}$.

Ministry of Railways , India, 1967, 1968 (4).

1967 Report: For Railway bridges in all parts of India for flow parallel to the pier, maximum scour depth occured at the nose and an average ratio of 'total scour depth' to Lacey depth of 1.71 was found.

1968 Report: (Scour around the piers of Ganga pul at Makameh). Average scoured depth at the nose of the piers gave a ratio of 1.75, whereas for an inclined attack scour along the sides averaged 2.15 $h_{s(Lacey)}$. It was observed that during non-monsoon floods the value of the ratio was larger, possibly due to a lower silt content, according the report. The corresponding values from 13 observations were 2.94 $h_{s(Lacey)}$ at the nose and 2.7 $h_{s(Lacey)}$ for scour along the sides of the piers. Measured scour depths during non-monsoon floods were slightly smaller, however, than during the largest monsoon flood.

1.3 Present Investigation:

From the above investigations two major approaches to the scour predictions are found. The first method mainly

aims at the prediction of maximum scour depth. In achieving this aim the attempt is to get a better prediction method by relating the various parameters to the scour mechanism. Contributors to this methodology are Tison (4), Keuthner (4), Posey (9), Laursen and Toch (6), Lacey (4), Inglis (4) and Arunachalum (4). In the second method, attempt has been made to understand the mechanics of the scouring process. Most of the studies attempted to relate the circulation of the horse-shoe vortex before scour with pier reynolds number, and other flow parameters relating to the circulation ratio. Strength of horse-shoe vortex is assumed constant during the scouring process. Based on the concept of constant strength of vortex, a model has been developed for scour predictions. In the study of this process, the major contributors are Baker (2) and Qadar (11), and Muzzammil (9).

In both these methods, no attempt has been made to study the change in flow mechanism during the scouring process. Further, the model developed by Baker violates the emperical conviction that the strength of vortex increases during the scouring process as Melvelli and Raudkivi's data predicts. Baker assumes that vorticity of the vortex decrease linearly with the increase in scour depth. There is a necessity to go into the details of understanding how vorticity decays during the scouring process, to achieve a

meaningful development of vortex scour model. This has been attempted in the present work.

CHAPTER 2

EXPERIMENTAL METHODS OF DATA COLLECTION

2.1 Details of Flume:

Two rectangular water flumes were used for the present investigation - one of 61 cm width and 8.0 m length while other one was 45 cm wide and 6.0 m long. The system of flow straighteners have been kept at the upstream end of the flume to get vortex free flow. The water has been supplied to the flumes from a overhead tank which get supply from the pumps. A calibrated rectangular weir has been used for measuring discharge passing through the flume. The test section for all experiments in both the flumes has been selected at 1.0 m upstream from the outlet. A cylinder 5.0 cm diameter and 30 cm height has been used as pier.

2.2 Details of Sediment Distribution:

Flume A was filled with sand of median size 0.50 mm and standard deviation 0.981 mm. Flume B was filled with sand of median size 0.145 mm and standard deviation 0.0154 mm. The size distribution of sand is shown in Fig. 2.1.

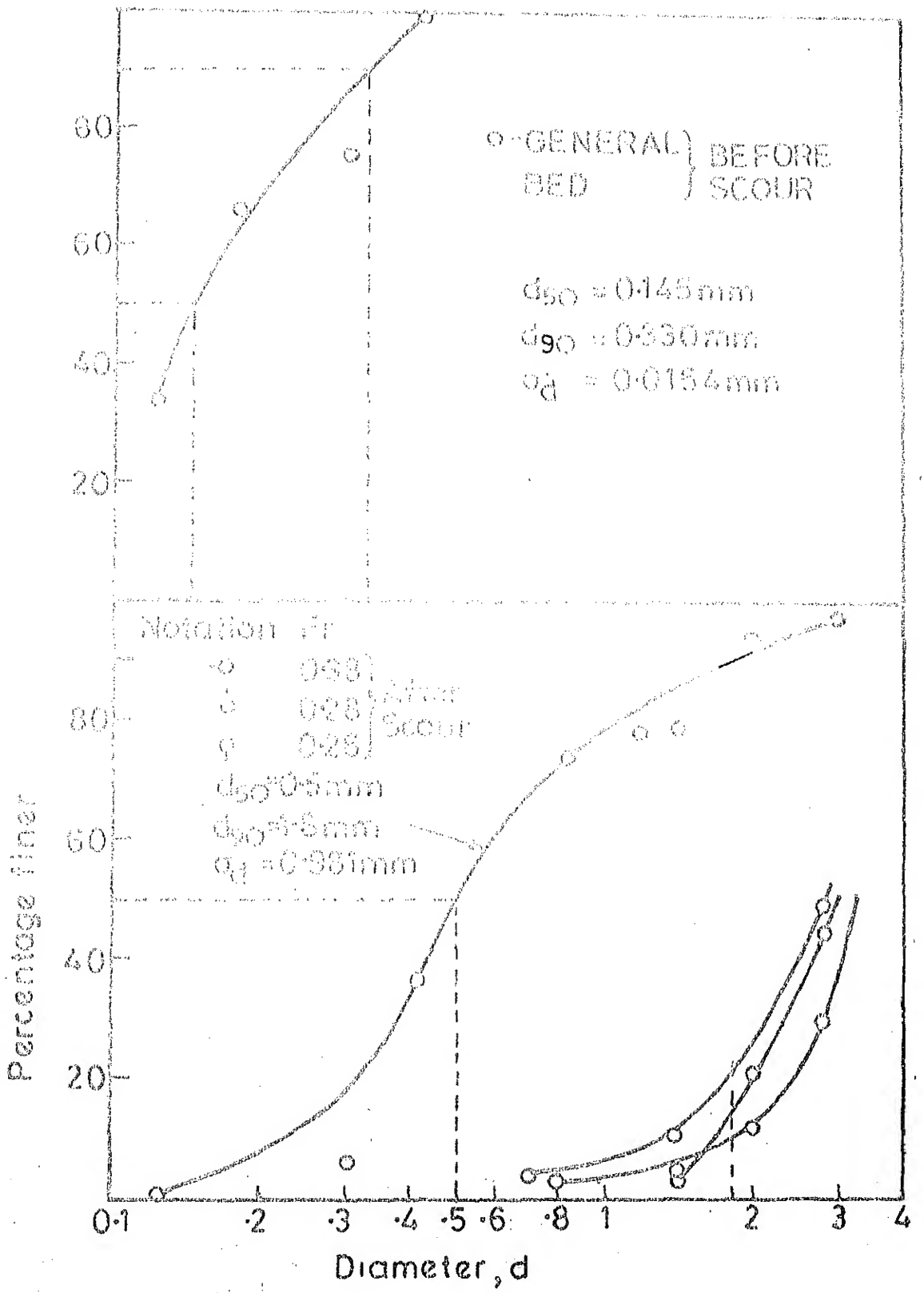

FIG.2.1 SEDIMENT SIZE DISTRIBUTION

2.3 Details of Flow Conditions:

Four experiments at different Froude numbers (one at incepient condition, two at pre-incepient conditions and one at post-incepient condition) were conducted in 'Flume A' .Every experiment was run for 4-5 hours till the scouring process attained an equilibrium condition. Table 2.1 shows the details of flow conditions.

Three experiments at different Froude numbers (one at incepient, one at pre-incepient and one at post-incepient condition) were conducted in 'Flume B'. The experiments were run till the scouring process attained an equilibrium condition. Table 2.2 shows details of flow run in 'Flume B'.

TABLE 2.1: DETAILS OF FLOW CONDITIONS IN FLUME A

Flume A: d_{50} = 0.50 mm, σ_d = 0.981 mm; Average Temp = 31°C; Kinematic viscosity = 7.86×10^{-7} m^2/sec.

Run No.	Symbol	Q in $m^3/s \times 10^{-3}$	h_o cm	δ cm	$\bar{U}$ cm/sec.	U_o cm/sec.	Fr.	Re $= U_o D/\nu$ $\times 10^4$
1	○	27.08	14.33	9.5	30.98	32.85	0.26	2.09
2	◑	15.60	9.53	6.9	26.84	29.71	0.28	1.89
3	◔	25.81	11.75	8.2	32.30	35.17	0.335	2.15
4	●	31.10	12.17	9.6	42.00	48.52	0.383	3.09

TABLE 2.2 : DETAILS OF FLOW CONDITIONS IN FLUME B.

Flume B	d_{50} = 0.145 mm	Average Temp = 27°C
	σ_g = 0.015 mm	Kinematic viscosity, ν = 8.0×10^{-7} m^2/sec

Run No.	Symbol	Q in m^3/sec $\times 10^{-3}$	h_o cm	δ	$\bar{U}$ c/s	U_o c/s	Fr	$R_e = U_o D/\nu$ $\times 10^4$
5	○	2.34	6.30	6.0	6.8	18.53	0.11	1.36
6	△	3.28	6.52	5.4	10.93	22.15	0.14	1.38
7	▽	9.10	8.47	6.3	23.88	28.01	0.24	1.75

2.4 Scour Measurements with Time:

The scour depth has been measured from the starting of scouring process to the moment when it appeared to attain an equilibrium condition, after interval of 1,2,5,10,20,30, 60,120, 180, 240, 300 minutes. Fig. 2.2A shows the plots between scour depth and time for the first four runs. Fig.2.2B shows scour depth plotted against time for the last three runs. The rates of scour with time (dh_s/dt) at different time intervals,stated above, were computed from these plots and have been shown in Table 2.3 and Table 2.4. The values of dimensionless scour rate (non-dimensionalized by U_o)are also shown in the table.

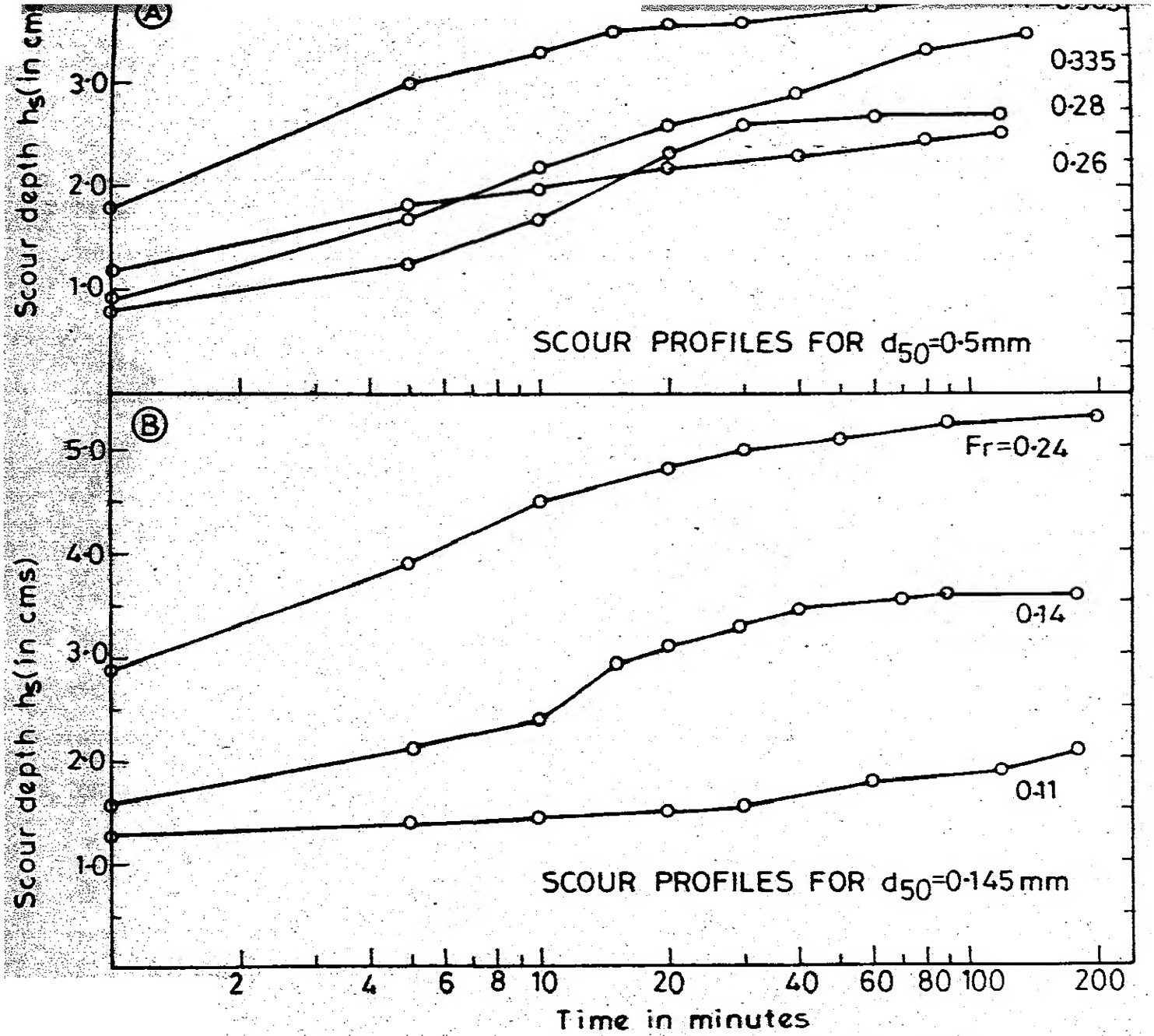

FIG. 2·2 SCOUR DEPTH PLOTTED AGAINST TIME

TABLE 2.3 : SCOUR RATES FOR RUNS IN FLUME A

Time (min.)	Run 1 (Fr = 0.26)		Run 2 (Fr = 0.28)		Run 3 (Fr =0.335)		Run 4 (Fr=0.383)	
	$\frac{\Delta h_s}{\Delta t} \times 10^{-5}$ (sec)	$\frac{\Delta h_s}{\Delta t} \times \frac{1}{U_o}$ $\times 10^{-6}$	$\frac{\Delta h_s}{\Delta t} \times 10^{-5}$ (sec)	$\frac{\Delta h_s}{\Delta t} \times \frac{1}{U_o}$ $\times 10^{-6}$ (Sec.)	$\frac{\Delta h_s}{\Delta t} \times \frac{1}{U_o}$ $\times 10^{-5}$	$\frac{\Delta h_s}{\Delta t} \times \frac{1}{U_o}$ $\times 10^{-6}$	$\frac{\Delta h_s}{\Delta t} \times 10^{-5}$ (sec)	$\frac{\Delta h_s}{\Delta t} \times \frac{1}{U_o}$ $\times 10^{-6}$
1	333.30	101.00	333.30	112.00	541.70	154.00	500.00	103.20
5	151.50	46.00	138.90	47.00	199.30	56.00	246.20	50.40
10	116.70	36.00	46.30	15.60	119.00	34.00	83.30	17.20
15	-	-	-	-	-	-	26.00	5.36
20	83.30	25.30	31.30	10.50	55.60	15.70	-	-
30	34.70	10.60	-	-	-	-	8.33	1.72
40	-	-	8.33	2.80	22.50	6.40	-	-
60	2.98	0.89	-	-	-	-	7.58	1.56
80	-	-	2.33	0.77	10.40	2.98	-	-
90	-	-	-	-	-	-	6.41	1.32
120	3.47	1.06	4.12	1.40	4.12	1.18	-	-

TABLE 2.4: SCOUR RATES FOR RUNS IN FLUME B

Time (min)	Run 5 (Fr = 0.11)		Run 6 (Fr = 0.14)		Run 7 (Fr = 0.24)	
	$\frac{\Delta h_s}{\Delta t} \times 10^{-5}$ (sec.)	$\frac{\Delta h_s}{\Delta t} \times \frac{1}{U_o} \times 10^{-5}$	$\frac{\Delta h_s}{\Delta t} \times 10^{-7}$ (sec)	$\frac{\Delta h_s}{\Delta t} \times \frac{1}{U_o} \times 10^{-6}$	$\frac{\Delta h_s}{\Delta t} \times 10^{-5}$ (sec)	$\frac{\Delta h_s}{\Delta t} \times \frac{1}{U_o} \times 10^{-6}$
1	41.70	224.9	208.3	94.1	416.7	148.7
5	16.70	89.9	161.3	72.8	250.0	89.3
10	5.60	30.0	138.9	62.7	107.1	38.2
15	-	-	-	-	-	-
20	5.60	30.0	100.0	45.1	41.7	14.9
30	13.80	74.9	41.6	18.8	17.8	6.35
40	-	-	29.8	13.4	-	-
60	8.33	44.9	-	-	8.8	3.15
90	-	-	10.4	4.7	5.6	1.98
120	3.85	20.8	-	-	0.88	0.31
180	3.03	16.3	0.0	0.0	-	-

2.5 Details of Velocity Measurements at the U/S:

The velocity measurements of the flows at about 1m u/s of the cylinder along the line of symmetry were recorded with the help of a pitot tube. The shear velocity, $V* (=\sqrt{\tau_o/\rho}$, where τ_o is the bed shear stress) has been computed assuming logarithmic velocity distribution namely,

$$\frac{u}{V*} = \frac{1}{\varkappa} \ln y + \text{constant}$$

where y is the ordinate measured from the bed, $\varkappa$ is Karman's constant taken equal to 0.4.

Figure 2.3 shows the details of shear velocity computations for all the runs and details of velocity measurements are shown in Table 2.5.

2.6 Velocity and Pressure Distribution in the Scour Hole:

Measurement of velocities within the scour hole at equilibrium condition, was done with the help of a mini-current meter along the centre line of the flume as well as along the depth of flow. Minicurrent meter (Type No. 7625), developed at Central Water and Power Research Station Poona, India, is capable of measuring the speed of water in the range of 5 cm/sec to 100 cm/sec. The propeller having 5 vanes, revolves at a speed linearly proportional to that of flowing water. The revolutions are counted by electro-mechanical counter.

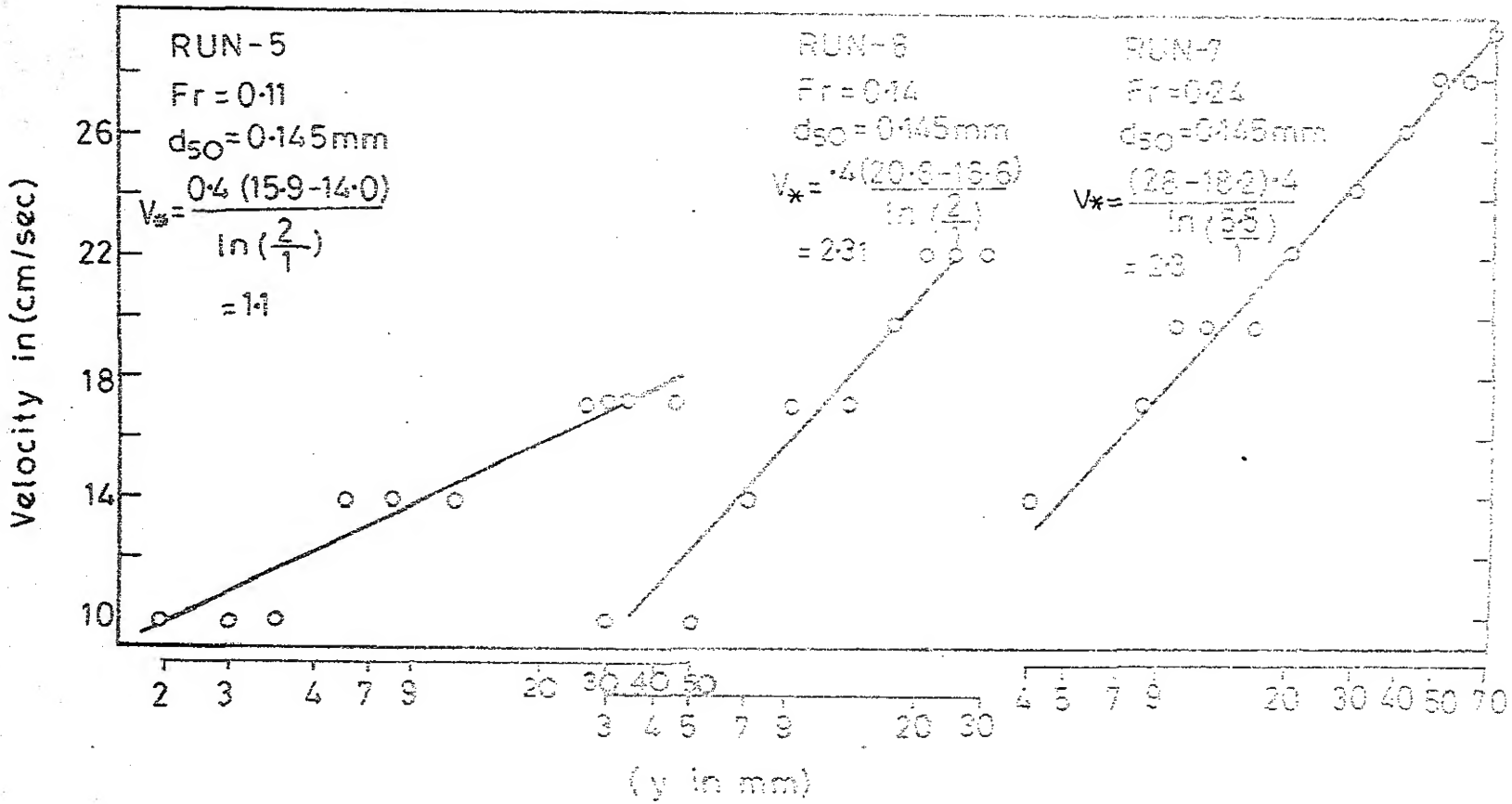

FIG.2.3A SHEAR VELOCITY COMPUTATIONS FOR d_{50}=0·145mm

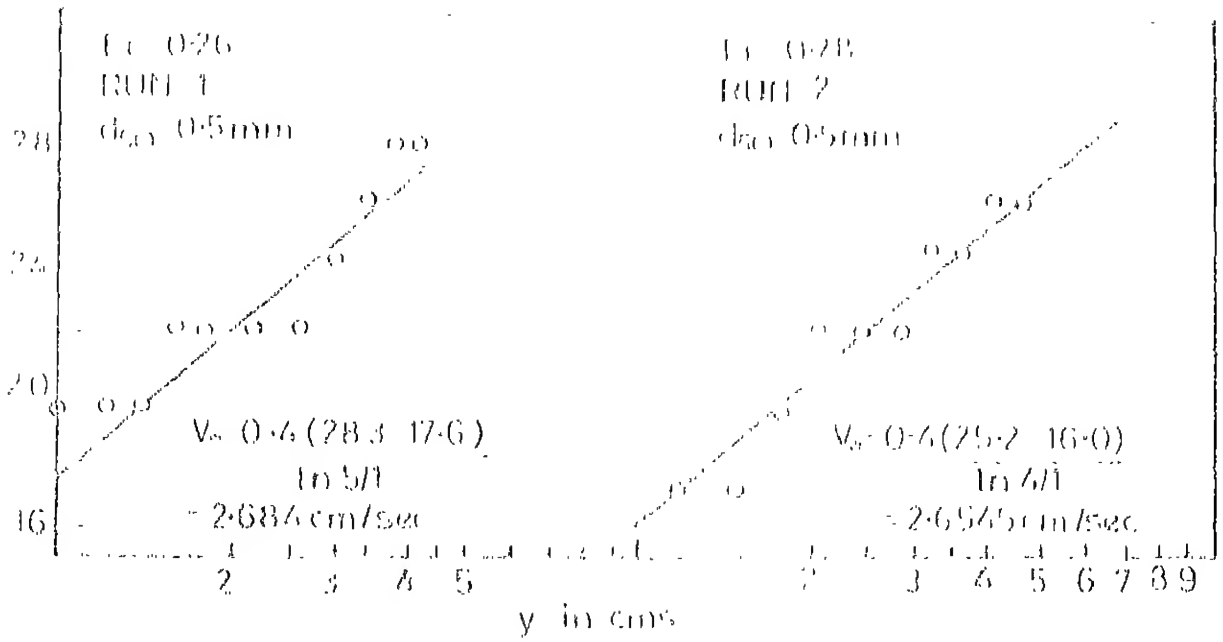

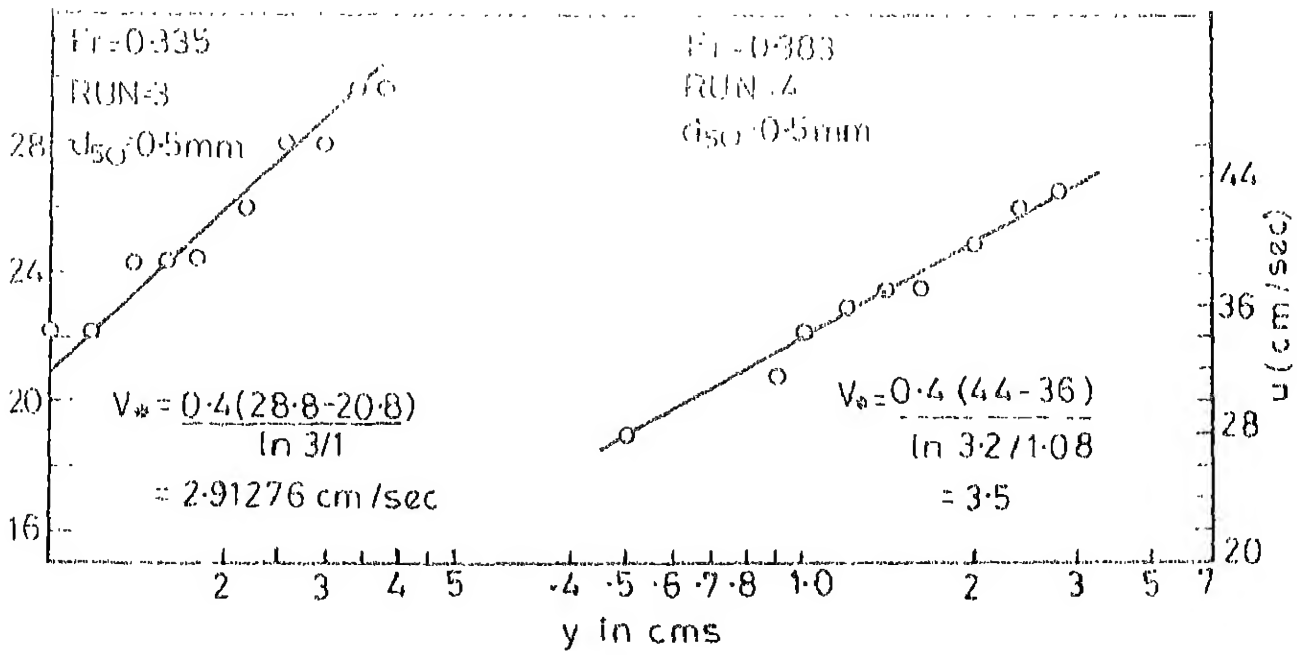

FIG.2·3B SHEAR VELOCITY COMPUTATIONS FOR d_{50}=0·5mm

TABLE 2.5 : DETAILS OF VELOCITY MEASUREMENTS

Run 1		Run 2		Run 3		Run 4		Run 5		Run 6		Run 7	
y, cm	u cm/sec.	y	u	y	u	y	u	y	u	y	u	y	u
0.3	9.90	0.5	9.90	0.3	9.90	0.3	19.15	0.3	9.90	0.3	9.90	0.20	0.00
0.5	14.00	0.7	9.90	0.5	14.00	0.5	22.14	0.5	9.90	0.5	9.90	0.40	14.01
0.7	14.00	0.9	14.00	0.7	14.00	0.7	22.14	0.7	14.00	0.7	14.00	0.60	17.16
0.9	17.15	1.1	17.20	0.9	17.15	0.9	24.30	0.9	14.00	0.9	17.20	0.80	19.80
1.3	19.80	1.3	19.80	1.3	19.80	1.1	28.30	1.3	14.00	1.3	17.20	1.40	19.80
1.7	22.14	1.6	19.80	1.7	22.14	1.3	31.30	1.7	14.00	1.7	19.81	1.80	19.80
2.3	22.14	1.9	22.14	2.3	24.30	1.5	34.30	2.7	17.20	2.1	19.81	2.80	22.14
3.1	24.30	2.2	24.30	3.1	26.20	1.9	34.30	3.7	18.53	2.5	19.81	4.80	24.26
3.9	28.00	2.6	24.30	3.5	28.00	2.4	35.70	4.7	18.53	3.0	19.81	5.80	23.01
4.7	29.70	3.0	24.30	3.9	29.70	2.4	35.70	6.2	18.53	6.4	19.81	6.80	28,01
5.5	29.70	3.4	26.20	4.3	30.80	3.9	37.10					7.80	28.01
6.3	29.70	4.8	26.20	4.7	31.30	4.9	38.40					8.40	28.01
7.3	28.00	5.3	28.00	5.2	32.85	5.9	39.60						
8.3	29.70	6.3	29.00	6.9	32.85	6.9	39.60						
9.3	31.30	7.3	29.70	7.2	34.30	7.9	40.34						
10.3	31.30	8.3	29.70	8.2	35.70	8.9	42.00						
11.3	32.35	9.3	29.70	9.2	35.70	9.9	43.20						
12.3	32.85			10.2	35.70	10.9	44.30						
End	31.30			11.7	35.70	11.9	48.5						

Pressures within the scour hole were measured with the help of a probe, details of which have been shown in Fig. 2.4. The average value of pressures measured at a distance of about 1.0 m upstream of the cylinder has been used as a reference pressure.

Figs. (3.15 & 3.16) shows the velocity contours velocities having been non-dimensionalized.

2.7 Details of Vorticity Probe, Vorticity Measurement:

Details of the vorticity probe used in the experiments are shown in Fig. 2.4. The vanes are made of very thin foil so that their inertia is minimum possible. The friction at the hinges has been reduced to its minimum. The number of rotations per minute (r.p.m.) made by vane assembly (rotor) have been counted by naked eyes after an interval of 1,5 , 10, 20, 40, 60, 120, 180, 240 minutes. These counts have been directly adopted as vorticily readings. These rotations were recorded at the location where rotor was judged to rotate fastest, i.e., centrally located in the horse-shoe vortex. Very small and thin pieces of flourescent tape were pasted on the same side of both the vanes so that it could be possible to count the number of rotations, seeing from above the water surface.

The details have been given below.

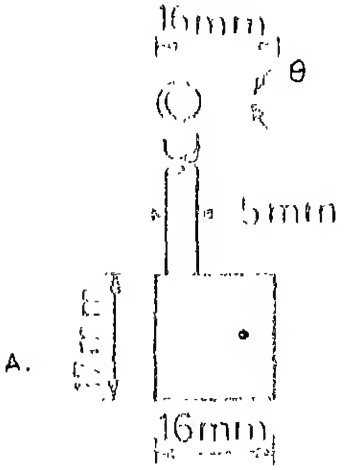

A.

Aagle $\theta = 16^{\circ}$

Dia. of hole = 1mm

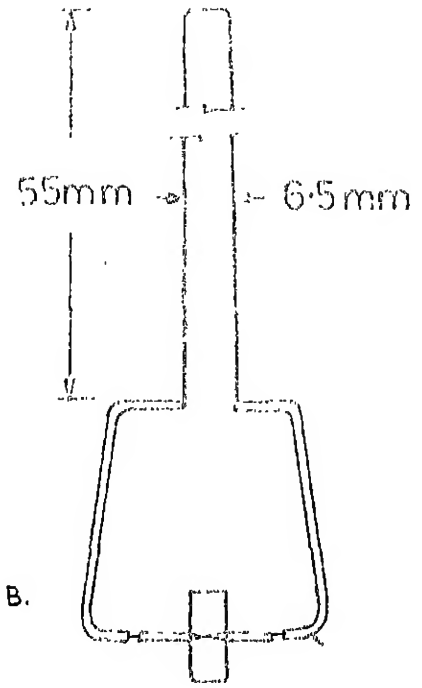

B.

Size of one vane = 3x5 mm

Dia. of axis about which two vane assembly rotates = 03mm

Dia. of Perifarial rod = 1mm

FIG·2.4 A. STATIC PRESSURE PROBE
B. VORTICITY PROBE

FLUME A	d_{50}	d_{90}	$V_{*c}(50)$	V_{*c}
	0.5 mm	1.8 mm	1.635 c/s	3.178 c/s

RUN: 1

Fr = 0.26

V_* = 2.6842 cm/sec

h_o = 14.33 cm

$\bar{U}$ = 30.98 cm/sec.

V_o = 32.85 cm/sec.

t (min)	$\frac{h_s}{D}$	ω (r.p.m.)
1	0.16	91
5	0.26	88
10	0.34	86
20	0.46	82
30	0.52	76
60	0.54	80

RUN: 2

Fr = 0.28

V_* = 2.6545

h_o = 9.53 cm

$\bar{U}$ = 26.84 cm/sec.

U_o = 29.71 cm/sec.

t (in min.)	h_s/D	ω (r.p.m.)
1	0.24	85
5	0.36	82
10	0.40	79
20	0.44	75
40	0.46	72
80	0.46	72

RUN: 3

Fr = 0.335

$V*$ = 2.91276

h_o = 11.75 cm

$\bar{U}$ = 32.30 cm/sec

U_o = 35.17 cm/sec.

t (in min.)	h_s/D	ω (r.p.m.)
1	0.18	98
5	0.34	96
10	0.44	95
20	0.52	87
40	0.58	86
80	0.67	80
140	0.70	76
200	0.69	72

RUN : 4

Fr = 0.383

$V*$ = 3.492

h_o = 10.48 cm

$\bar{U}$ = 42.00 cm/sec.

U_o = 48.52 cm/sec.

t (in min.)	h_s/D	ω (r.p.m.)
1	0.36	103
5	0.60	98
10	0.66	86
15	0.71	73
30	0.72	70
60	0.75	64
90	0.78	64

FLUME B	d_{50}	d_{90}	$V_{*c(50)}$	$V_{*c(90)}$
	0.145 mm	0.33 mm	1.182 cm/s	1.385 cm/s

RUN: 5

Fr = 0.11

V_* = 1.02

h_o = 6.30 cm

$\bar{U}$ = 8.60 cm/sec

U_o = 18.53 cm/sec.

t (in min.)	h_s/D	ω (r.p.m.)
1	0.26	23
5	0.28	22
10	0.28	25
20	0.30	28
30	0.31	33
60	0.32	27
120	0.38	25
180	0.42	24

RUN: 6

Fr = 0.14

V_* = 2.31

h_o = 6.52 cm

$\bar{U}$ =10.93 cm/sec

U_o =22.15 cm/sec

t (in min.)	h_s/D	ω (r.p.m.)
1	0.32	31
5	0.38	43
10	0.48	46
15	0.59	35
20	0.62	34
30	0.66	27
40	0.69	21
60	0.71	20
120	0.73	18

RUN: 7

Fr = 0.24

V_* = 2.30

h_o = 8.47

$\bar{U}$ =23.88

U_o =29.01

t (in min.)	h_s (in cms)	ω (r.p.m.)
1	2.9	20
5	3.9	24
10	4.5	28
20	4.8	33
30	5.0	45
60	5.1	43
90	5.25	36
120	5.30	36

Analysis of vorticity of vortex, as it sinks with the scour hole development has been analysed in the next chapter. Prior to this, analysis vortex strength and size before initiation of scour has been made from the data available in literature.

2.8 Sediment Size Distribution in the Deepest Portion of the Scour Hole:

The sediment grains have been collected from the deep portion of the scour hole by pressing the plastic clay on the scoured surface. Sieve analysis has been carried out for these sediment samples. Sieve analysis data for three runs on sand of median size 0.5 mm and the original bed sample sieve analysis data for both the sands have been plotted in Fig. 2.1.

CHAPTER 3

CHARACTERISTICS OF VORTEX

Characteristics of vortex studied are the position of vortex in scour hole, vorticity decay and strength of vorticity before the initiation of the scour. These characteristics of vortex are studied using the data available in literature. Data of Melville and Raudkivi, C.J. Baker, A.K. Gupta, Qadar were analysed. The vorticity data collected from two median size sands beds are analysed in the light of the analysis of the data available in literature. Static pressure distributions and velocity distributions in the scour hole are also presented and discussed.

3.1 Analysis of Data Available in Literature:

Characteristics of vortex, like positions of centre of vortex , scales of the major and minor axis of the ellipitical shaped vortex, in a scour hole are computed using Melville and Raudkivi's data.

3.1.1 Positions of centre and scales of vortex in a scour hole:

Fig. (3.1) shows the magnitudes and directions of mean velocity past a 5.08 cm diameter cylinder in the vertical plane of symmetry ahead of the cylinder for the initial, intermediate and equilibrium conditions as obtained by Melville and Raudkivi. These data were obtained from a 45 cm wide glass sided flume filled with sand having a uniform grading curve with d_{35} = 0.30 mm, d_{50} = 0.385 mm, d_{65} =0.500 mm and a specific gravity of 2.65. A flow of 17.12 l/s was used and it yielded on the bed slope of S_o = 0.0001 a uniform flow depth h_o = 0.15 m and a mean approach velocity 0.25 m/s. The shear velocity, V_* was 1.21 cm/sec. They found that increases from the initial flat bed value at $\Gamma = 7.91 \times 10^{-5}$ m^2/s to $\Gamma = 9.02 \times 10^{-3}$ m^2/s (at h_s/D = 0.923) for the intermediate scour to $\Gamma = 1.19 \times 10^{-2}$ m^2/s (at h_s/D = 1.32) for the equilibrium scour hole in the plane of symmetry ahead of the cylinder.

From the Fig. (3.1), it is observed that the vortex plunges down into the scour hole, with its tangential velocities along the different elliptical paths remaining the same, as

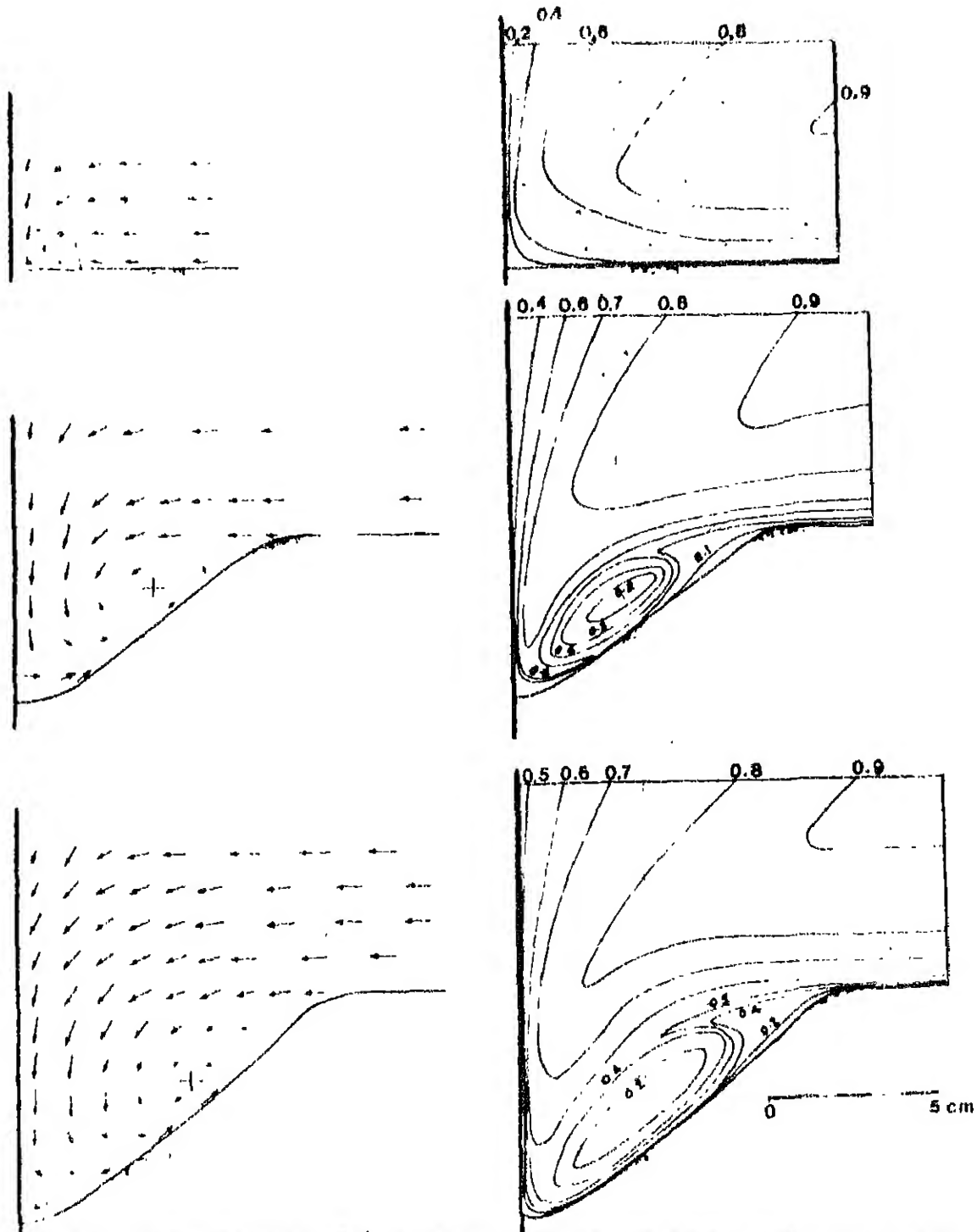

Fig. 3.1: Direction(left) and magnitude of mean velocity part a 50.8 mm diameter pier in the vertical plane of symmetry ahead of the cylinder for the initial flat bed condition (top), the intermediate scour hole and the equilibrium scour hole condition (bottom). (8)

scour progresses. The horse-shoe vortex assumes an elliptical shape in the scour hole. The major axis of this elliptical vortex stretches with the development of scour, whereas the minor axis remains fairly the same.

The position of the centre of the vortex in the scour hole is measured and given in Table (3.1) . 'X' is the perpendicular distance of the centre from a surface of cylinder; 'Y' is its depth below the initial bed level and 'Z' is its distance along the major axis, from the point where the sloping armoured bed meets the cylinder.

TABLE 3.1 : POSITION OF CENTRE OF VORTEX

Condition	X (cm)	X/D	Y (cm)	Y/D	Z (cm)	Z/D	h_s (cm)	h_s/I
Interme-diate scour hole	3.13	0.62	2.34	0.46	3.76	0.74	4.68	0.9
Equilibrium Scour hole	3.80	0.74	3.28	0.65	4.98	0.98	6.72	1.3

It may be observed that the vortex centre moves away from the surface of the cylinder. The ratio of depth of vortex centre from initial bed level to the scour depth remains consta and is approximately 1/2.

By measuring the perimeter of the constant velocity contours of these vortices, the vorticity,ω, has been computed as follows:

For a circular vortex, the strength of vortex, can be written as

$$\Gamma = \omega r \ (2\pi r)$$

where r is the radius of circular path of a fluid element in the vortex.

Non-dimensionalizing and writing in terms of perimeter, P_e

$$\frac{\Gamma}{UD} = \frac{\omega D}{U 2\pi^2}\left(\frac{2\pi r}{D}\right)^2 = \frac{1}{2\pi^2}\frac{\omega D}{U}\left(\frac{P_e}{D}\right)^2 \qquad \ldots (3.1)$$

For an elliptical vortex,

Γ = (velocity of ellipical path) (perimeter of this pat

or, $\Gamma = V\theta \cdot P_e$

substituting the value of Γ in the above equation (3.1) an expression for ω can be written after simplification as

$$\frac{\omega D}{U} = \frac{2\pi\left(\frac{V_\theta}{U}\right)}{\left(\frac{P_e}{D}\right)}$$

or $$\omega = 2\pi\left(\frac{V_\theta}{P_e}\right)$$

P_e/D is measured for given values of V_θ/U_θ, and vorticity is computed and tabulated as shown in Table (3.2) below.

TABLE 3.2: VALUES OF ω FOR INTERMEDIATE AND EQUILIBRIUM SCOUR HOLE

Condition	Velocity Contour (V_θ/U_θ) (1)	Perimeter (in cms) (2)	Velocity, U (in cm/sec) (3)	$\omega = \frac{(3)}{(2)} \times 2\pi$ (r.p.s.
Intermediate Scour Hole	0.2	17.33	5.0	1.81
	0.3	26.67	7.5	1.77
	0.4	33.33	10.0	1.89
Equilibrium Scour Hole	0.2	34.67	5.0	0.906
	0.4	48.00	10.0	1.31

It can be concluded from the above table that an average the vorticity remains fairly constant along the different elliptical (tangential velocity) paths for a particular position of the vortex. This can be seen clearly in the case of intermediate scour hole condition. This confirms that the vortex is of forced type. Magnitude of vorticity decreases from intermediate scour hole condition to equilibrium scour hole condition.

Figure (3.2) shows the tangential velocity distribution along major and minor axes for the intermediate scour hole and the equilibrium scour hole. The width scale of the vortex is chosen when the tangential velocity starts decreasing. These width scales, non-dimensionalized with the pier diameter D, are plotted against h_s/D in Fig. (3.4B).

From the figure, it is clear that the minor axis scale 'b', remains fairly constant (b/D = 0.2) whereas the major axis scale a increases with increase in scour depth. The increase is not linear but appears to be varying as square of h_s/D. The following equation may be given.

$$\frac{a}{D} = \frac{a_o}{D} + \frac{1}{3.3}(h_s/D)^2 \qquad (3.2)$$

Perimeter scale of the vortex is computed and plotted in the Fig. (3.3). It may be observed that the growth rate of vortex perimeter scale in the order of $(h_s/D)^{5/2}$. The following equation may be given

$$\frac{P_e}{D} = \frac{P_{e_o}}{D} + \frac{1}{3}\left(\frac{h_s}{D}\right)^{5/2}$$

The computed vorticity (Table 3.2) nondimensionalized with the initial vorticity is plotted against h_s/D for intermediate scour hole and equilibrium scour hole. The decay of the vorticity is very fast, of the order of $(h_s/D)^6$, as can be seen from Fig. (3.3).

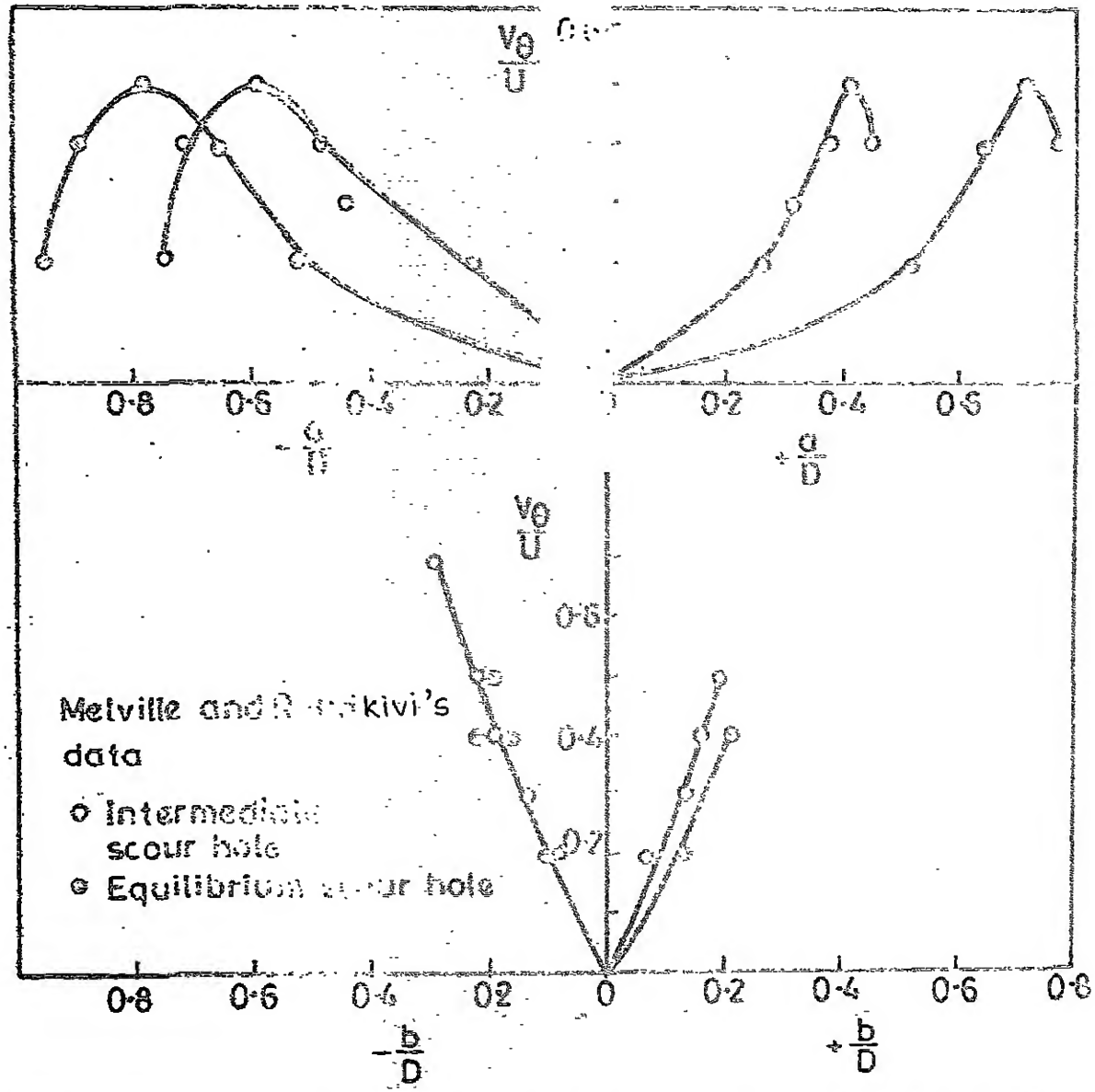

FIG. 3.2 MAJOR AND MINOR AXES SCALE OF VORTEX PLOTTED AGAINST V_θ/U

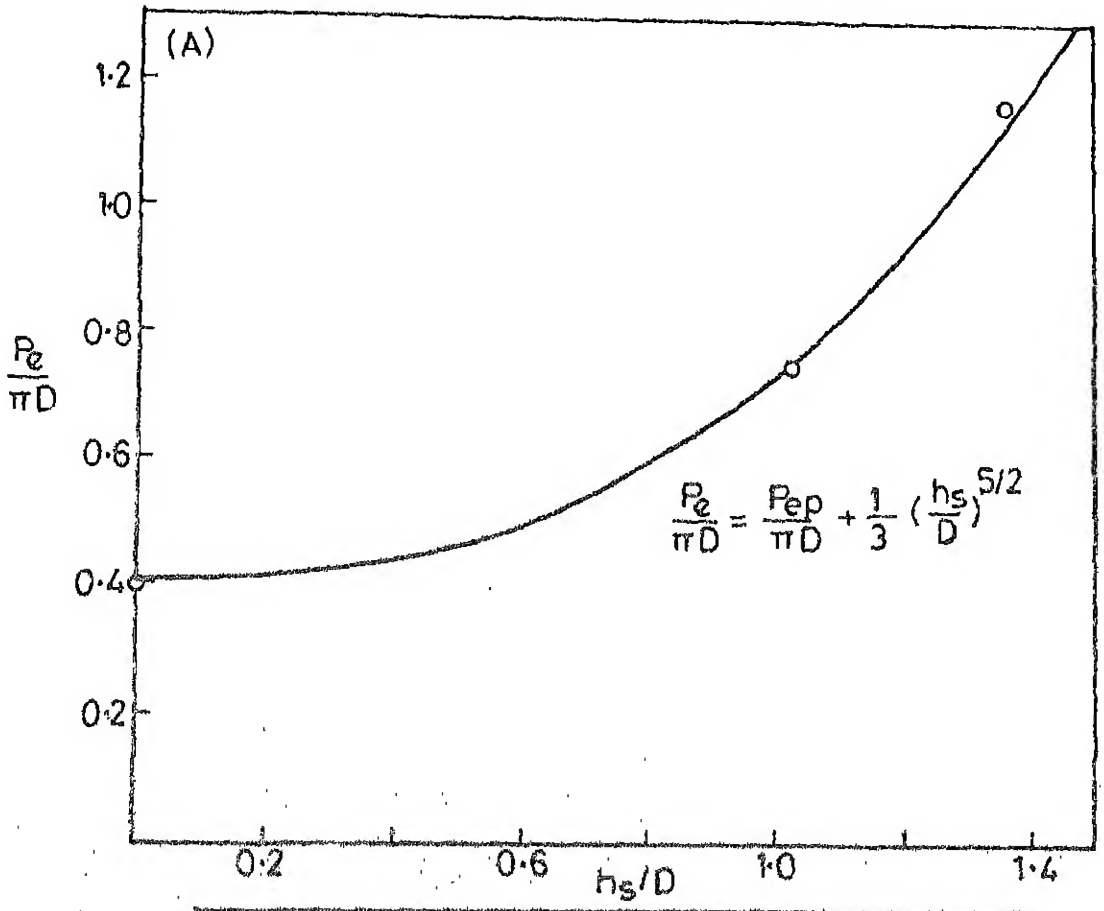

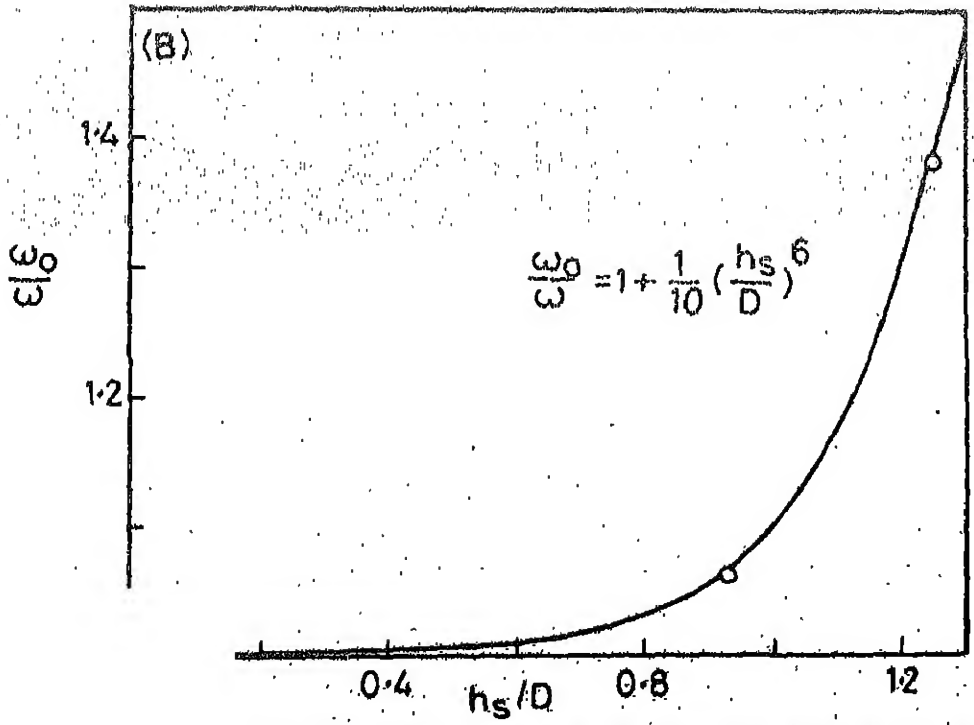

PRIMETER SCALE PLOTTED AGAINST SCOUR DEPTH, h_s

DECAY OF VORTICITY WITH SCOUR DEPTH, h_s

Strength of vortex, non-dimensionalized with initial vortex strength, is plotted against h_s/D in Fig. (3.4A). It increases directly with h_s/D as can be seen in figure.

Some important conclusions drawn from the detailed analysis of Melville and Raudkivi's data, have been summarised below.

1. The horse-shoe vortex sinks into the scour hole with scour progress and assumes the shape of an ellipse.
2. The centre of vortex is located at a half of the scour depth.
3. Minor axis of the ellipse remains unchanged while major axis increases very fast with the increase in scour depth.
4. The vorticity along different elliptical paths of vortex is of forced type.
5. Vorticity decays with increase in scour depth.
6. Vortex strength increases with increase in scour depth.

3.1.2 Initial vortex strength computations:

It is essential to know the initial vortex strength characteristics because of their importance in the scouring process. With this view, the data of Gupta (5), Muzzommil (9), Baker (1) and Qadar (11) are analysed.

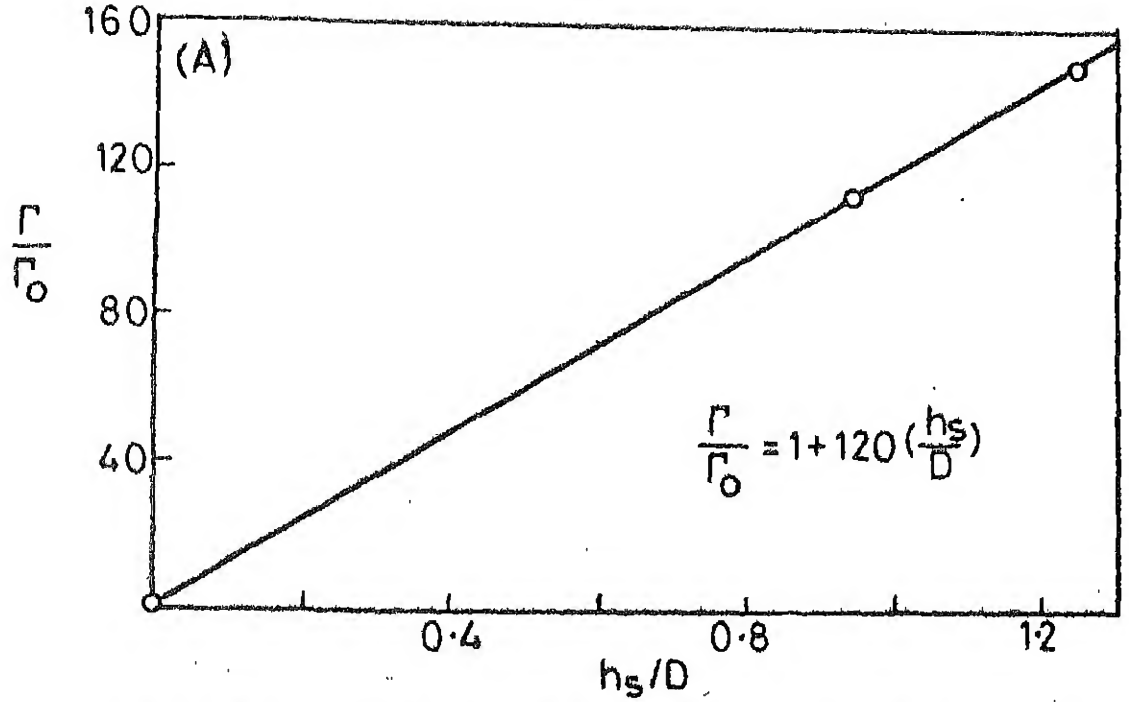

FIG. 3.4A VORTEX STRENGTH VARIATION WITH SCOUR DEPTH

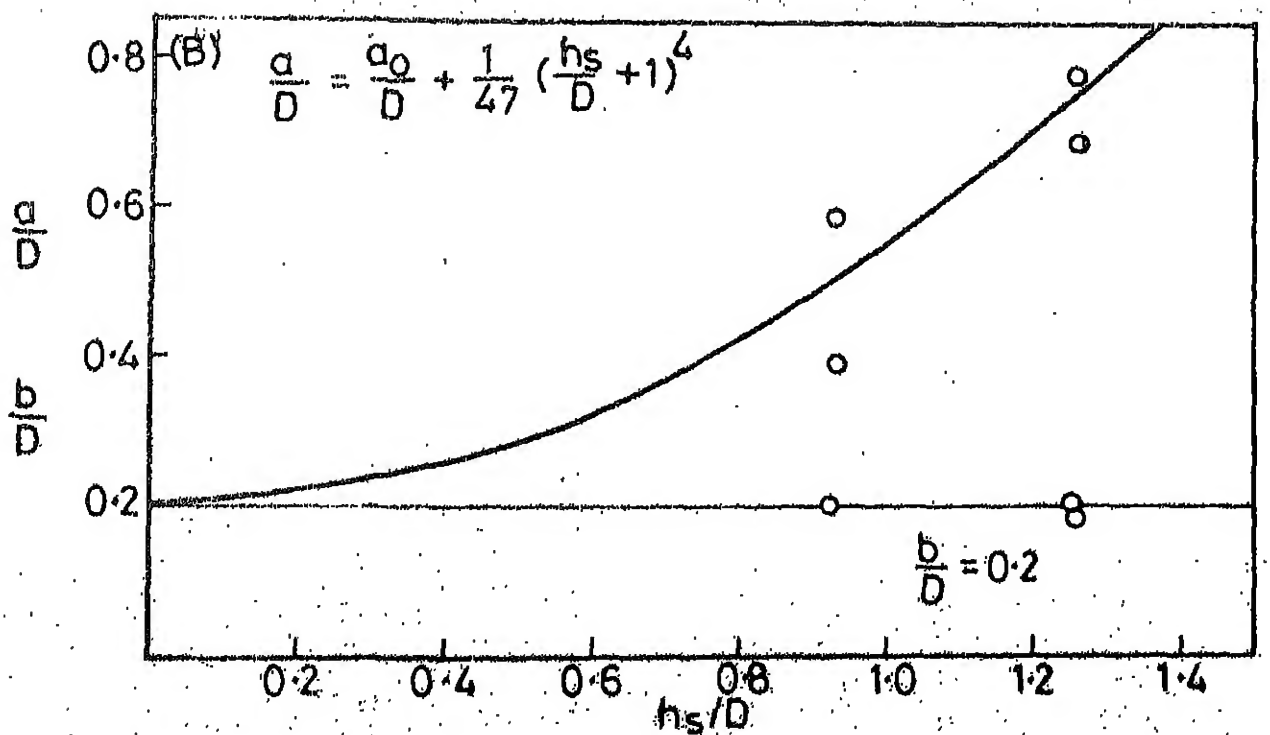

FIG. 3.4B VARIATION OF MAJOR AND MINOR AXES WITH SCOUR DEPTH, h_s

The vortex strength is computed from the pressure profiles measured on the rigid bed along the line of symmetry upstream of the cylinder. The method followed is that of Gupta. It was observed that one or more depressions exist on the pressure profile at the location of vortices. This fact is utilized in the computation of vortex strength. As vortices are of forced types, having crest with edge of the vortex and through with the centre of the vortex, strength of each vortex must be proportional to the pressure difference between the crest and through of a depression or a valley. The following formula was derived by Gupta (5):

$$\frac{\Gamma_o}{\pi D U_o} = \left(\frac{2\Delta r}{D} \right) (\Delta C_p)^{1/2} \qquad (3.3)$$

where ΔC_p = Difference in pressure coefficients between edge and centre of the vortex.

Δr = distance on the plate between edge and centre of the vortex.

ΔC_p and Δr have been shown in a schematic figure below.

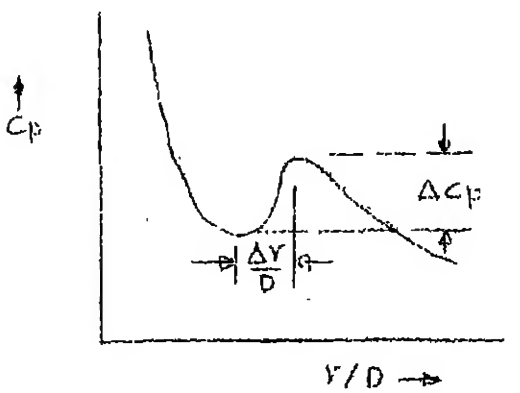

The wind tunnel data of Gupta, for boundary layer depths (δ/D) varying from 0.5 to 2.0, are used. The data of Muzzammil's experiments, conducted in water flume for the same diameter of pier as has been used for the present investigation, were analysed. Baker's (1) data, collected from wind tunnel experiments for laminar as well as turbulent flow, have also been analysed. A. Qadar's data collected from water flow in a flume were analysed. From all the data, $\Gamma_o/D\bar{U}$ is computed and plotted in Fig. 3.5 against Pier Reynolds number $\bar{U}D/\nu$ where $\bar{U}$ is mean velocity of flow, D is pier diameter, and ν is kinematic viscosity.

Here, it is necessary to check the validity of the computation with measured values of strength of vortex (non-dimensionalized with '$\pi D\bar{U}$'). For this, velocity profiles measured by Baker and Qadar have been used. The computation procedure is described below.

Fig. (3.6) shows plots between rotational velocity (non-dimensionalized with maximum velocity) and non-dimensionalized length along the axis on which velocities were measured.

$$\text{Now, } \frac{\Gamma_o}{\pi D\bar{U}} = (V_{\theta_o})\, 2\pi r \times \frac{1}{\pi D\bar{U}} = \left(\frac{V_{\theta_o}}{\bar{U}}\right).\left(\frac{2r}{D}\right)$$

The values of $(V_{\theta_o}/\bar{U})$ and $(2r/D)$ have been shown in an illustrative figure drawn below. In this figure D is diameter of cylinder equal to 7.6 cm for Baker's data. D varies from 2.54 cm to 10.16 cm in case of Qadar's data.

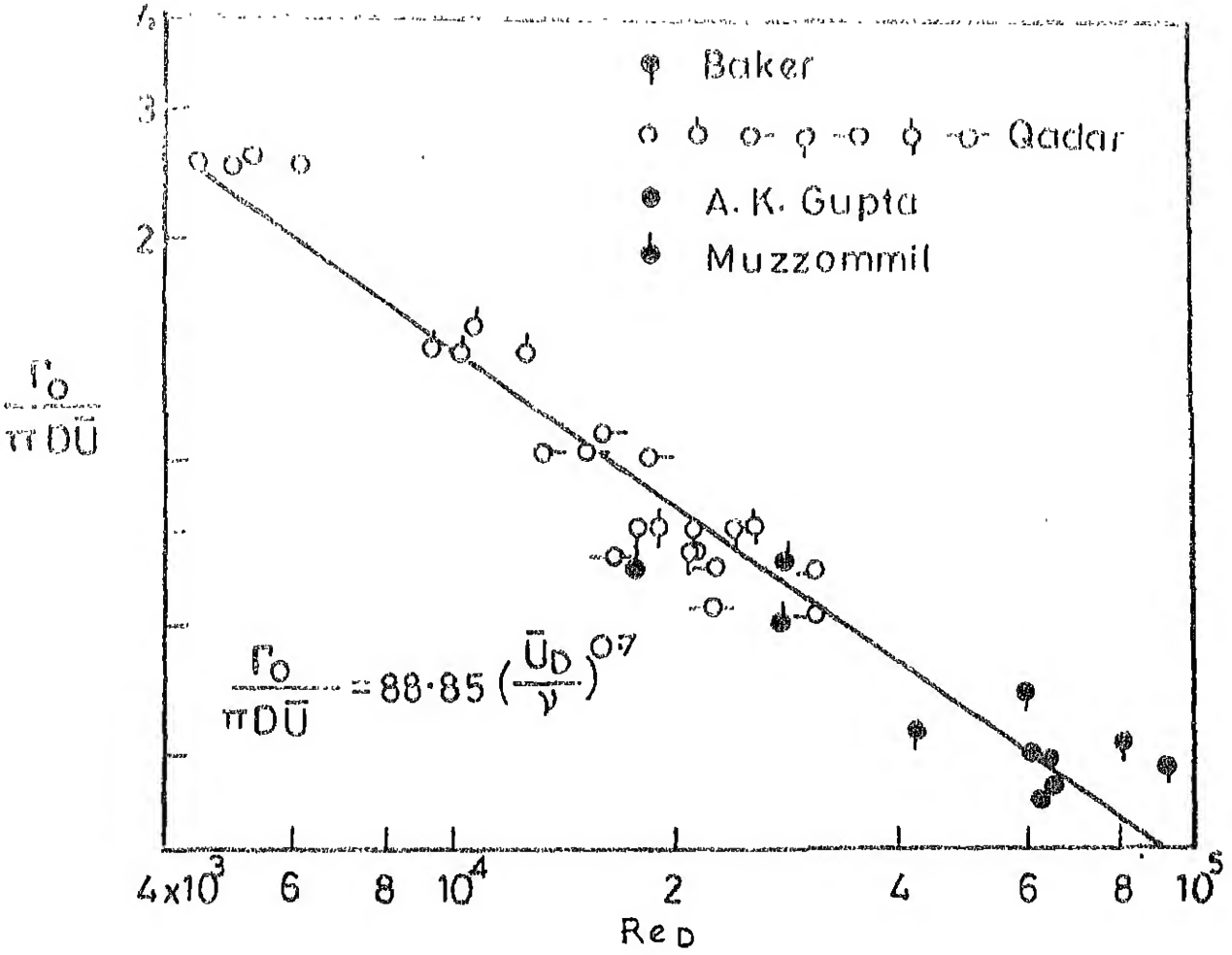

FIG. 3.5 RELATION BETWEEN VORTEX STRENGTH AND Re_D

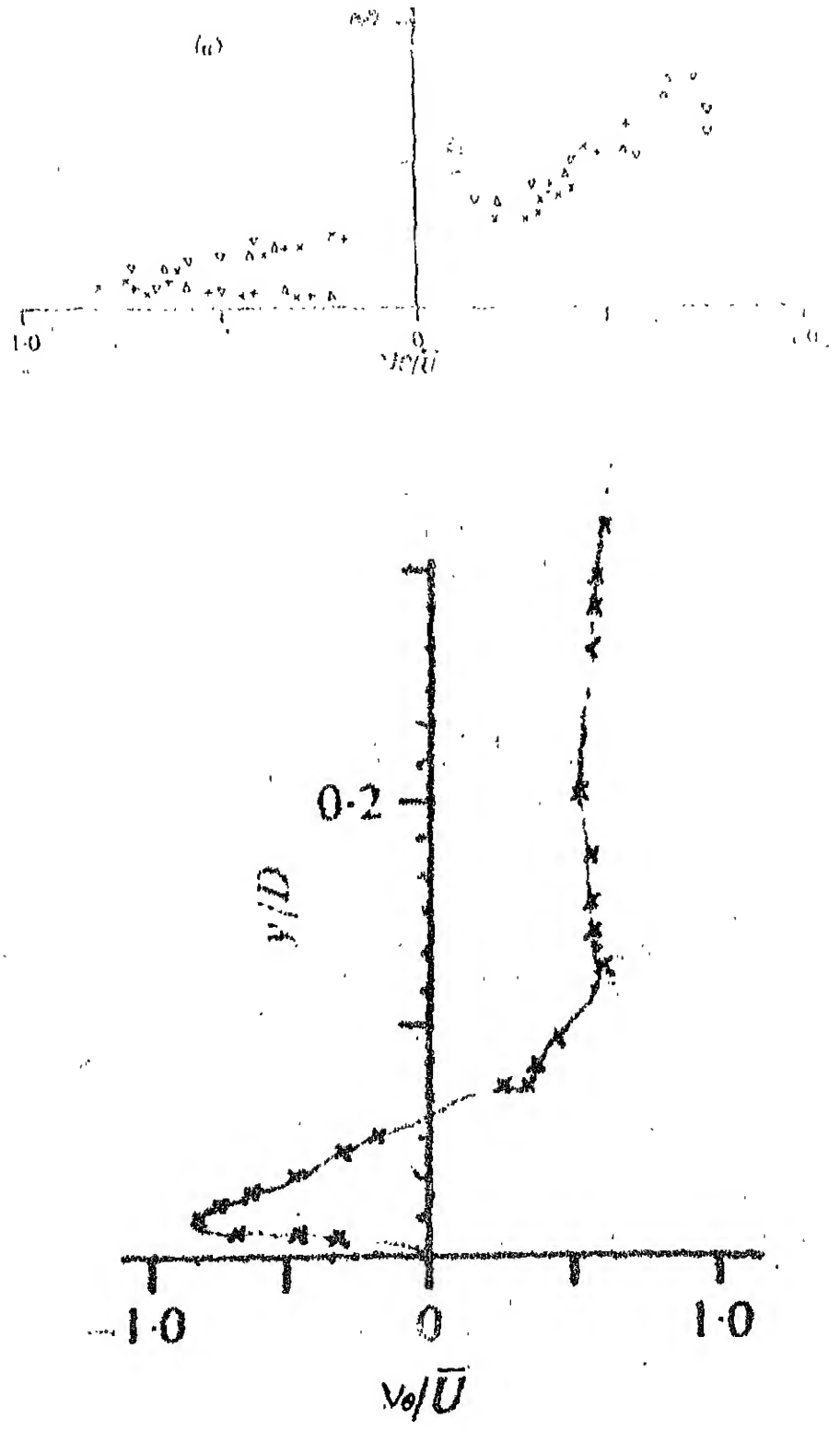

Fig. 3.6: Plot between rotational velocity and length of axis as obtained by Baker (1)

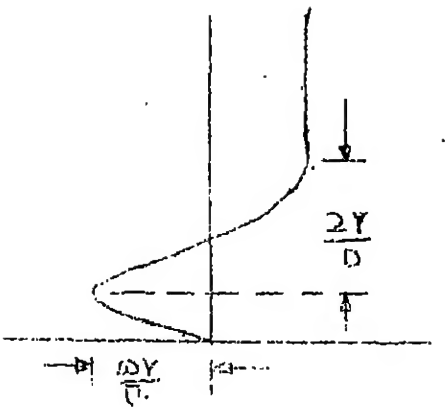

SCHEMATIC DIAGRAM SHOWING VALUES OF (2r/D) and ($\omega r/\bar{U}$)

These computed data are also plotted in the Fig. (3.5) It may be observed that the data points, computed from pressure profiles, concide with the data points computed from velocity profiles. Hence we conclude that the method of computation suggested by Gupta may be considered appropriate.

The initial vortex strength $\Gamma_o/\pi D\bar{U}$ decreases with increase in Reynolds number as is clear from the Fig. (3.6). The following empirical relations for $\Gamma_o/ D\bar{U}$ with pier Reynolds number, may be suggested

$$\frac{\Gamma_o}{\pi D\bar{U}} = 88.85\ (\bar{U}\ D/\nu)^{-0.7}$$

This leads to an important conclusion that the strength of initial vortex, formed in the separating region before scour, is a function of pier Reynolds number.

Using the velocity and pressure profiles, the size of the vortex is computed and plotted in (Fig.3.7) against

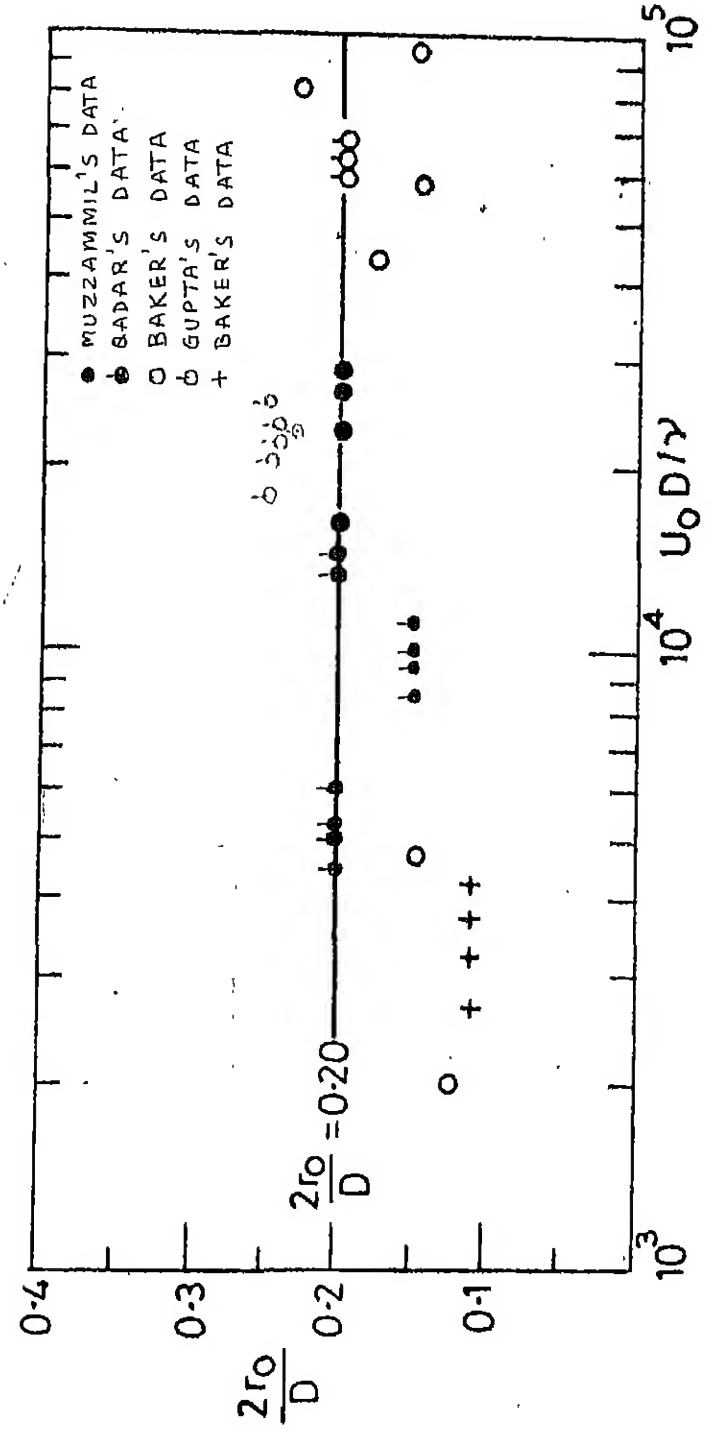

FIG.37 RADIUS OF VORTEX PLOTTED AGAINST REYNOLDS NUMBER

Pier Reynolds number $U_o D/\nu$. It may be observed that the size of the vortex remains constant at $2Y/D = 0.2$

Initial vorticity is computed from the Qadar's and Baker's data as follows:

$$\frac{\omega_o D}{\bar{U}} = \left(\frac{V_{\theta o}}{\bar{U}}\right)\left(\frac{D}{r_o}\right)$$

where V_{θ_o} is the maximum tangential velocity of vortex and r_o is the radius measured from the centre. For the data of Muzzammil and Gupta, initial vorticity is computed from the strength of horse-shoe vortex before scour as

$$\frac{\omega_o D}{\bar{U}} = \frac{r_o}{D\bar{U}} \cdot \frac{1}{2}\left(\frac{D}{r_o}\right)^2$$

Thus computed initial vorticity ω_o nondimensionalized with D and $\bar{U}$ as $\omega_o D/\bar{U}$ is plotted against Pier Reynolds number $(\bar{U}D/\nu)$ in Fig.(3.8). An empirical equation may be written as

$$\frac{\omega_o D}{\bar{U}} = 3.5 \text{ Exp } \left[- \left(\frac{R_{eD}}{65000}\right)^{1.14} \right] \qquad (3.4)$$

It may be observed that $\omega_o D/\bar{U}$ decreases with increase in Pier Reynolds number of the flow.

With these studies on the vortex characteristics before and during the scouring process, the vorticity measuremen

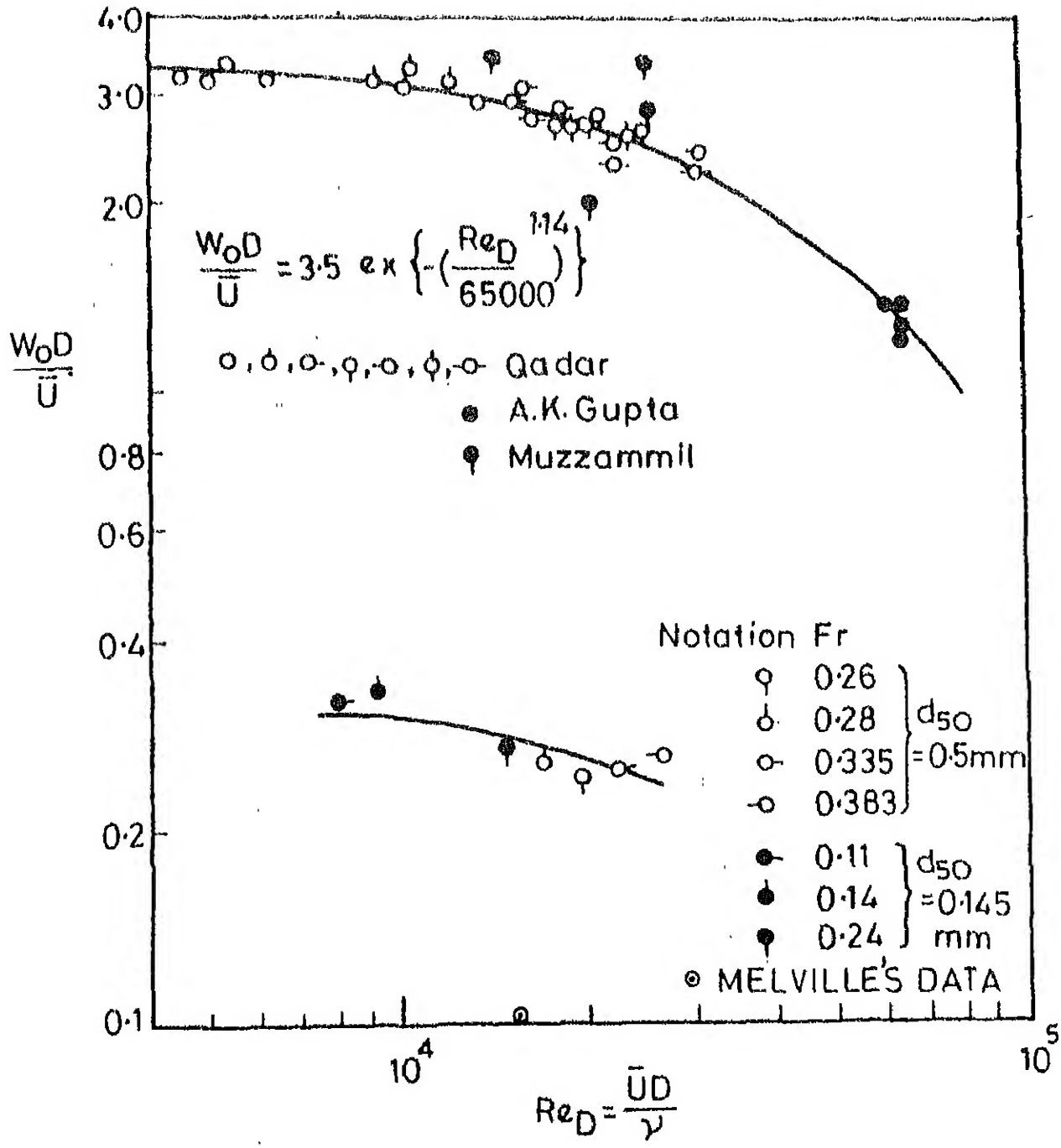

FIG. 3.8 $\frac{W_oD}{\bar{U}}$ PLOTTED AGAINST Re_D

made in the present work are analysed.

3.2 Vorticity Decay with Scour:

For the experiments with relatively coarse sand, i.e. , sand of median size 0.5 mm, vorticity decreased with increase in scour depth. This happened for all the runs of flow. But for experiments with finer sand, i.e., sand of median size 0.145mm vorticity first increased and then decreased in the same manner as in the case of coarse sand. This might have occured because of size of vorticity probe which was used for measuring the vorticity. In the initial stages, the width of the deepest portion, adjacent to the cylinder, for the finer sand is somewhat narrower and it was not possible to take the axis of the probe well with in the deepest portion. In the present analysis only receding limb data have been considered as they correspond to well developed scour hole.

Initial vorticity before the scour, could not be measured because once the cylinder is introduced as obstruction to the flow, the scouring is rapid and, hence, there is no time available for the measurement of the vorticity. Therefore, vorticity is measured after one minute from the start of scour. Tables(Art.2.7)summarises the measured vorticity data.

The vorticity is non-dimensionalized with pier diameter D and maximum velocity U_o as $\omega D/U_o$ and plotted against h_s/D as shown in Fig. (3.9). It can be observed

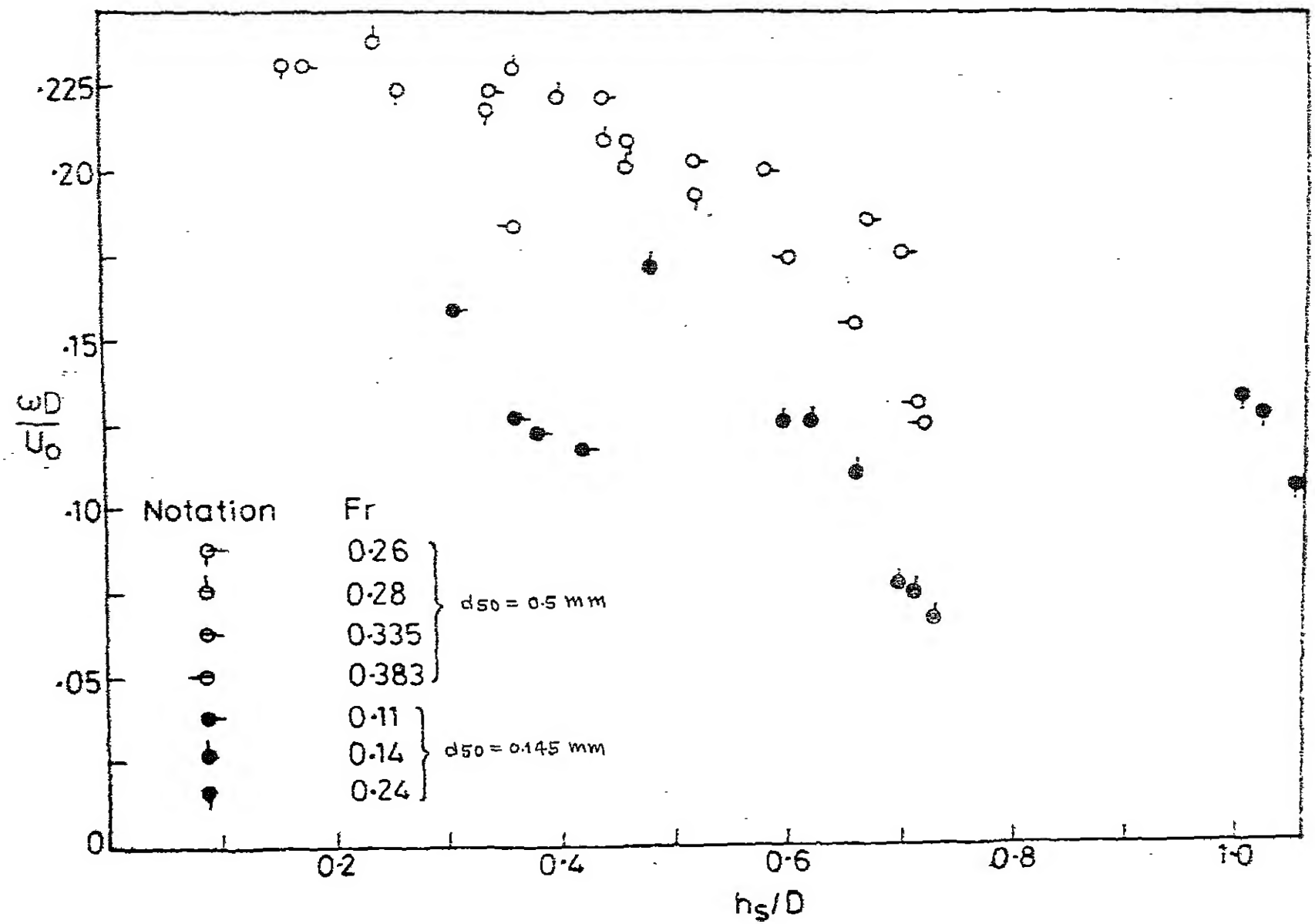

FIG. 3·9 VARIATION OF VORTICITY WITH SCOUR DEPTH

from the figure that the vorticity decays with increase in scour depth. The decay rate varies with one or more parameters which may be from among U_o, V_*, D, d_{50}, d_{90}, V_{*c}, $V_{*c(90)}$, h_o and δ. After an exhaustive analysis, taking various possible combinations, it was found that the parameter V_{*c}/U_o, gives a better corelation. The scour rate is written as $(\frac{D+h_s}{D})\ V_{*c}/U_o$. The scour scale $\frac{D+h_s}{D}$ is chosen because the major axis of the vortex increases with scour depth from its initial value corresponding to the size of initial vortex. The size of initial vortex is a function of pier diameter whereas the size of vortex at some intermediate scour is a function of both pier diameter and depth of scour. Also, to some extent $(\frac{h_s+D}{D})\ V_{*c(50)}/U_o$ represents the ratio of strength of the vortex considered to the strength of initial vortex. The Threshold velocity $V_{*c(50)}$, as per Shield's criterian, has been considered becauuse it represents the initiation of grain motion.

The vorticity $\omega D/U_o$ decays with $(\frac{h_s+D}{D})\ V_{*c(50)}/U_o$ as can be seen from Fig. (3.10). The decay is very gradual upto $(\frac{h_s+D}{D})\ V_{*c(50)}/U_o$ 1 0.05 but increases very fast with further increase in $(\frac{h_s+D}{D})\ V_{*c(50)}/U_o$. Here, it may be recalled that the vorticity computed from Melville and Raudkivi's data also decays very fast with scour process as can be seen in Fig. (3.3). An empirical relationship of vorticity decay may be written as follows:

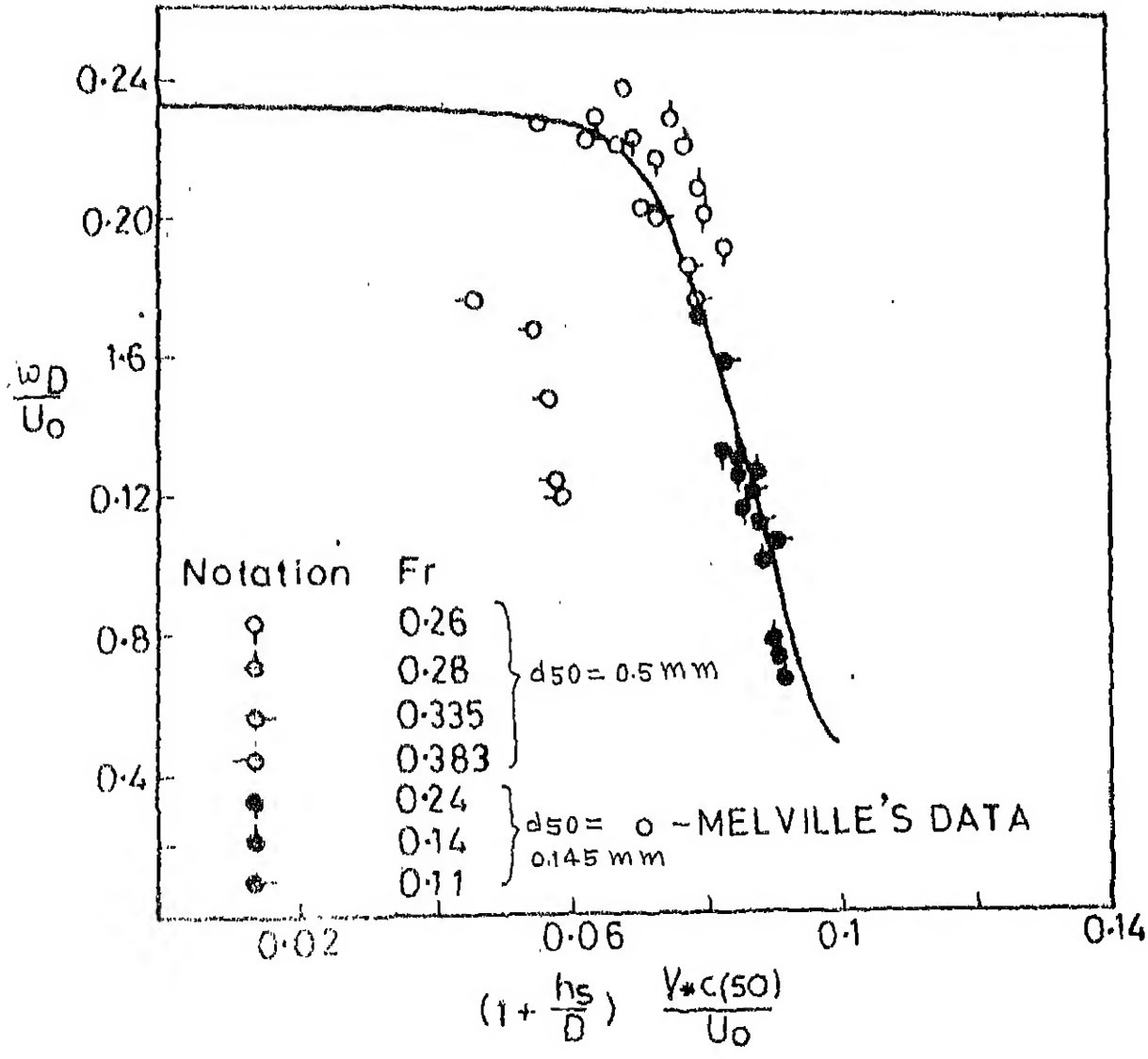

FIG. 5.10 DECAY OF VORTICITY WITH $(1+\frac{h_s}{D})\ \frac{V_{*c(50)}}{U_o}$

$$\frac{\omega D}{U_o} = \frac{1}{4.32 + \left[12.88 \left(1 + \frac{h_s}{D}\right) \frac{V_{*c(50)}}{U_o} \right]^{11}} \quad (3.5)$$

The vorticity of the initial vortex, ω_o is found to be a function of $V_{*c(50)}/U_o$, as per the above equation. This can be computed by putting $h_s/D = 0$ in the equation. The computed vorticity, non-dimensionalized with $\bar{U}$ and D is plotted in Fig. (3.8). The present study indicates that the vorticity values are, on an average, 0.1 times those obtained from Qadar, Muzzammil, Gupta and Baker's data for corresponding Pier Reynolds number. Initial vorticity data computed from Melville and Raudkivi's data is also plotted. This value is still lower when compared to the present study. This is somewhat strange and needs further investigation.

3.3 Rate of Scour:

Scour depth against time has been plotted in Fig. (3.11) for all the flow runs. It may be observed that the scouring rate is higher in the early period; decays gradually with increase in time, leading to the equilibrium of the scour depth after about 180 minutes.

Force equilibrium equation for the removal of sand grain from the scouring bed may be written as,

$$C_1 \frac{\pi d^2}{4} \rho \left[\omega D \frac{(h_s+D)^2}{D}\right] - C_2 \frac{\pi d^2}{4} \left(\frac{\rho_s-\rho}{2}\right) V_c^2 = C_3 \frac{\pi d^2}{4} \left(\frac{\rho_s-\rho}{2}\right) \left(\frac{dh_s}{dt}\right)^2 \quad ..(3.6)$$

In the above equation, the first term represents the fluid force due to tangential velocity of vortex acting

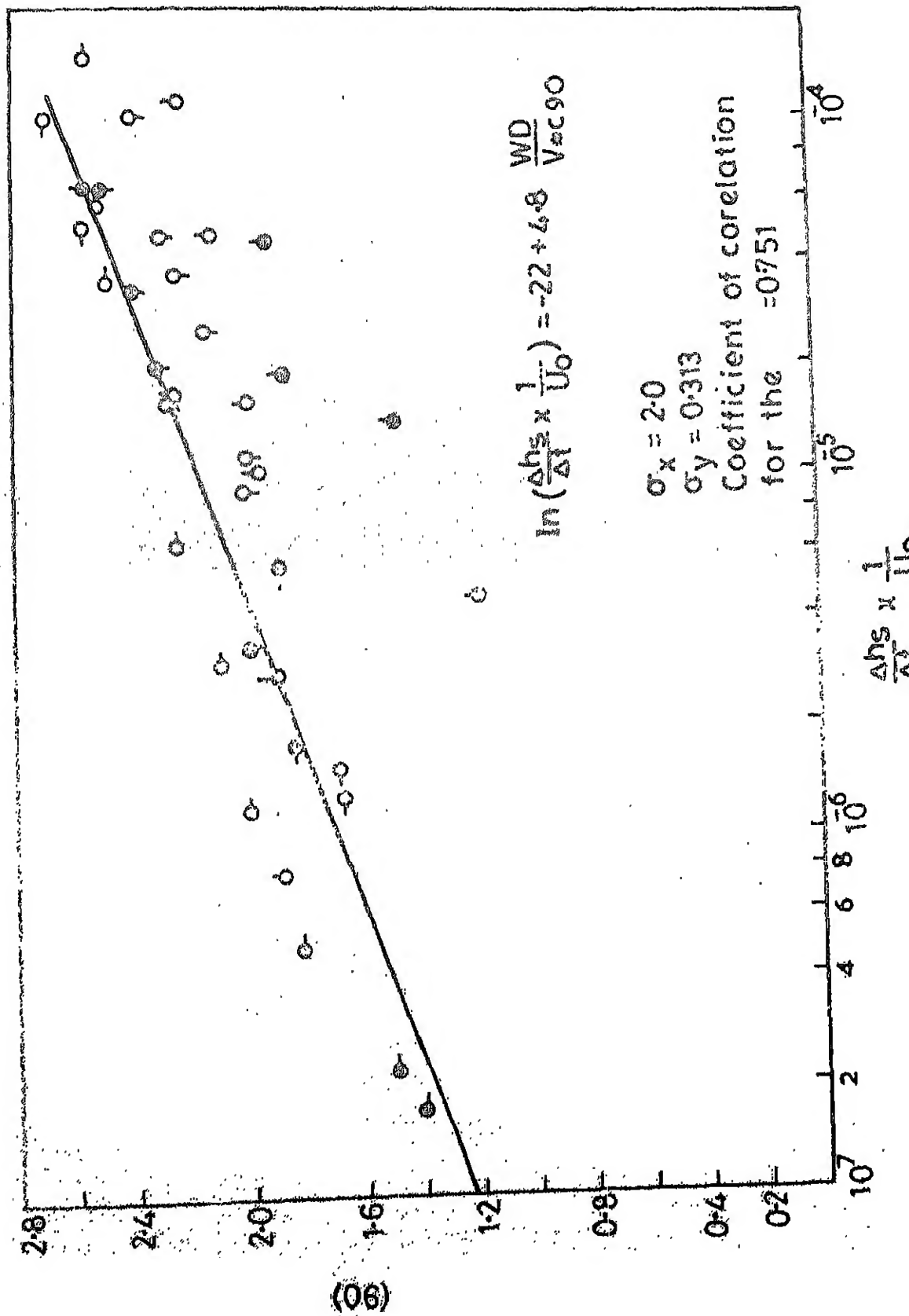

FIG.3·11 RATE OF SCOUR WITH VORTICITY

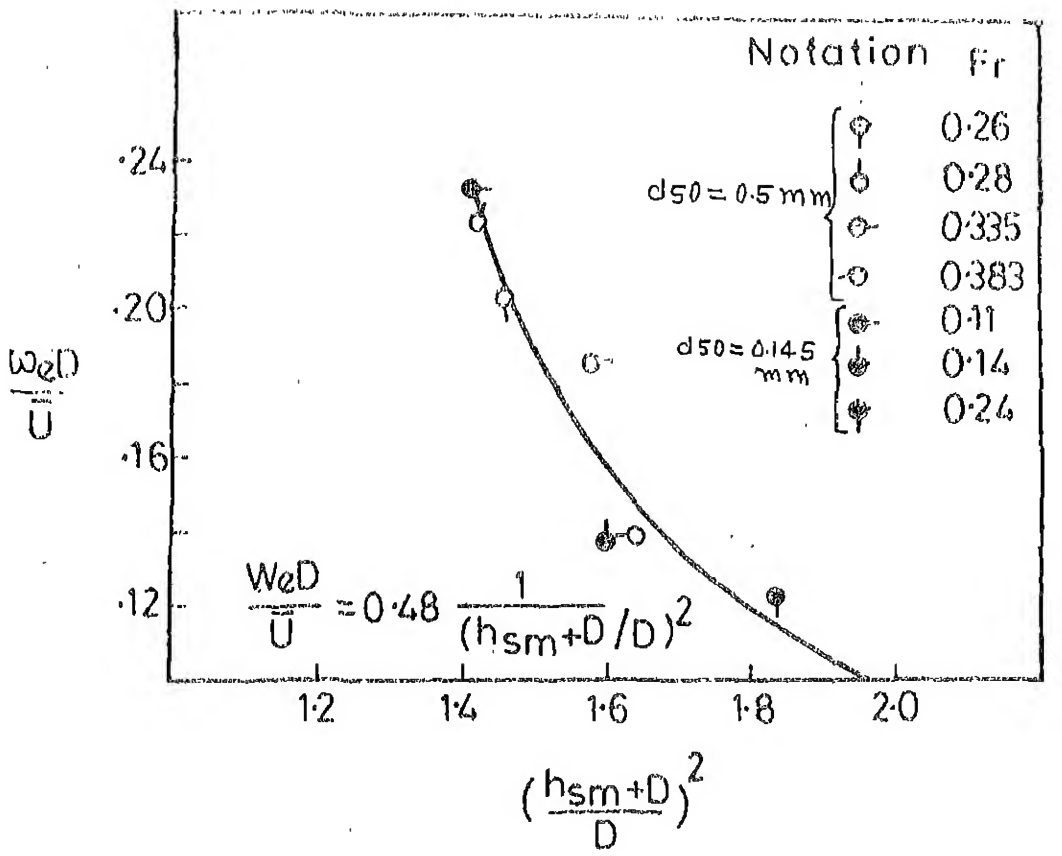

FIG·3·12 EQUILIBRIUM VORTICITY PLOTTED AGAINST MAXIMUM SCOUR DEPTH

In order to relate the equilibrium vorticity with initial vorticity ω_o, a plot of $\frac{\omega_e}{\omega_o}$ is made against the flow parameter $\frac{V_{*c(90)}\delta}{U_o D}$ in Fig. (3.13A). The flow parameter $\frac{V_{*c(0)}\delta}{U_o D}$ is chosen for the following reason.

$V_{*c(90)}$ is chosen because of the fact that median size, d_{50} of the sediment in the deepest portion of the scour hole corresponds to d_{90} of the sand filled in the flume as observed by Muzzammil (9). The parameter $V_{*c(9)}\delta/U_o D$ can be rewritten as

$\frac{V_{*c(90)}}{D}$ ~ Vorticity corresponding to equilibrium condition / Vorticity corresponding to vorticity before scour in the approaching flow.

$\frac{V_{*c(90)}}{D}$ ~ Minimum tangential velocity of the vortex corresponding to threshold velocity of d_{90} size / Corresponds to major diameter of the elliptical vortex at equilibrium condition.

The ratio of vorticities ω_e/ω_o increases with increase in $V_{*c(90)}\delta / U_o D$ and approaches to unity at large values of $V_{*c(90)}\delta/\omega_o D$. Following equation may be written as

$$\frac{\omega_e}{\omega_o} = 1 - \exp\left[-9.2 \frac{V_{*c(90)}\delta}{U_o D} \right] \qquad (3.11)$$

3.5 Comparision of Experimental Maximum Scour Depth with the Computed One:

In order to check the over all validity of equations derived so far in the present work, compression between experimental $(\frac{h_{sm}+D}{D})$ and computed values of $\frac{h_{sm}+D}{D}$ is being made.

From Eq. (3.11),

$$\frac{\omega_e}{\omega_o} = 1 - \exp\left[- 9.2 \frac{V_{*c(90)}\,\delta}{U_o\, D} \right] = A \text{ , say}$$

or
$$\frac{\omega_e D}{\bar{U}} = \frac{\omega_o D}{\bar{U}} \cdot A \qquad (3.12)$$

From Eq. (3.10),

$$\frac{\omega_e D}{\bar{U}} \left(\frac{h_{sm} + D}{D}\right)^2 = 0.48$$

or
$$\frac{\omega_e D}{\bar{U}} = \frac{0.48}{\left(\frac{h_{sm}+D}{D}\right)^2} \qquad (3.13)$$

equating right hand sides of Eq. 3.12 and Eq. 3.13

$$\frac{\omega_o D}{\bar{U}} A = \frac{0.48}{\left(\frac{h_{sm}+D}{D}\right)^2}$$

or
$$\frac{\omega_o D}{\bar{U}} = \frac{0.48}{A\left(\frac{h_{sm}+D}{D}\right)^2} \qquad (3.14)$$

Now, from Eq. (3.4) (drived using Qadar, Muzzammil, Gupta and Baker's data),

$$\frac{\omega'_o D}{\bar{U}} = 3.5 \exp\left[- \left(\frac{R_{eD}}{65000}\right)^{1.14} \right]$$

where $R_{e\,D} = \frac{\bar{U}D}{\nu}$, pier Reynolds number, ω'_o is vorticity computed from Eq. (3.4).

In the above equation, the value of vorticity is 10.0 times higher (please refer Art.3.2) than the value of vorticity for the present work, hence dividing R.H.S. by 10.0, one can get expression for $\omega_o D/\bar{U}$. Therefore,

$$\frac{\omega_o D}{\bar{U}} = 0.35 \text{ Exp } \left[- \left(\frac{R_{eD}}{65000} \right)^{1.14} \right] \qquad (3.15)$$

Equating right hand side of Eq. (3.14) and Eq. (3.15),

$$\frac{0.48}{A\left(\frac{h_{sm}+D}{D}\right)^2} = 0.35 \text{ Exp } \left[- \left(\frac{R_{eD}}{65000} \right)^{1.14} \right]$$

or,
$$\left(\frac{h_{sm}+D}{D}\right)^2 = \frac{1.37}{A} \text{ Exp } \left[\left(\frac{R_{eD}}{65000} \right)^{1.14} \right] \qquad (3.16)$$

Using above equation $(h_{sm}+D)/D$ are computed for different runs and compared with expdrimental $(h_{sm}+D)/D$ in Fig. (3.13B). It may be observed that the comparision between the two is fiar.

3.6 Vortex Strength Relationship

Another model for scour prediction based on vortex strength at equilibrium condition was proposed by Gangadharaiah, Muzzammil and K. Subramanya (13) . In this model the length of major axis of the vortex at equilibrium condition is taken proportional to $\left(\frac{h_{sm}+D}{D}\right)$. Also, tangential velocity of the vortex should be equal to threshold velocity $[V_{*c(90)}]$ of the sediment at the deepest portion of scour. Therefore, the strength of the vortex can be written as

$$\Gamma_e = K_1 \; V_{*c(90)} \; (D+h_{sm}) \qquad (3.17)$$

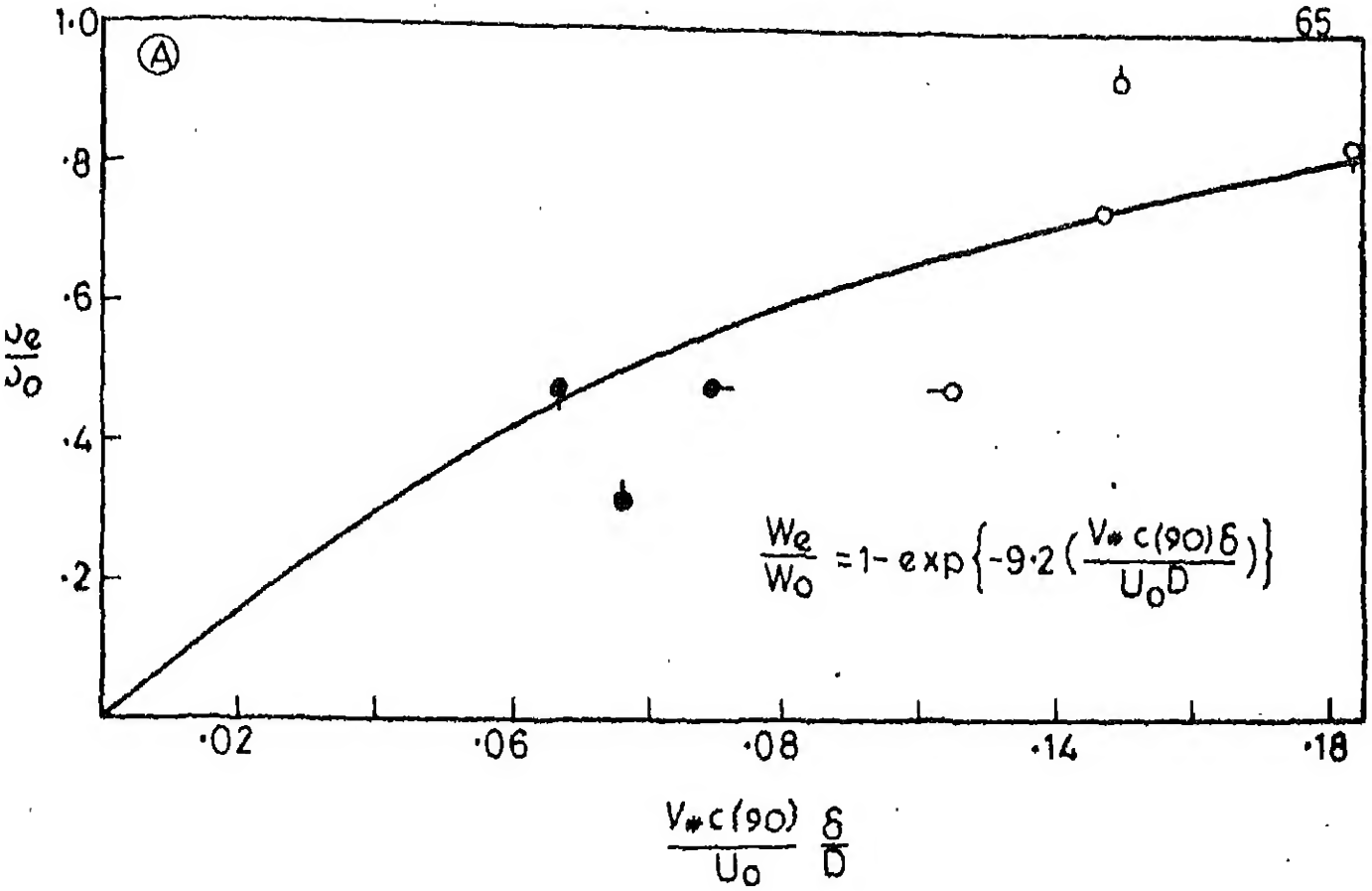

FIG. 3·13(A) DECAY OF VORTICITY

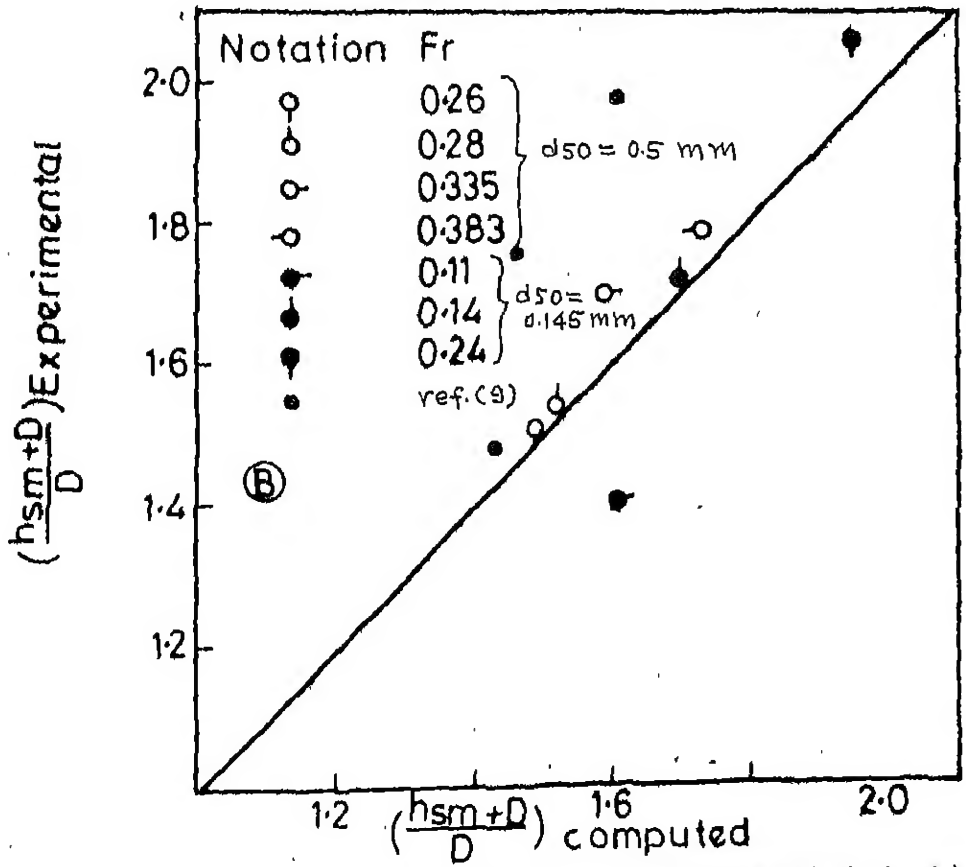

FIG. 3·13(B) COMPARISON OF EXPERIMENTAL AND COMPUTED RESULTS

Non-dimensionalizing with $V_* \delta$

$$\frac{\Gamma_e}{V_* \delta} = K \frac{V_{*c(90)}(D+h_{sm})}{V_* \delta} \qquad (3.18)$$

The vortex strength is plotted against the flow parameter $\frac{U_o D}{V_* \delta}$ in Fig. (3.14) and the variation expressed as

$$\frac{V_{*c}(D+h_{sm})}{V_* \delta} = 0.3 \left(\frac{U_o D}{V_* \delta}\right)^{0.84}$$

Experimental data of the present work are incorporated in the above model as shown in Fig. 3.14. It may be observed that the present data deviates from the curve proposed.

3.7 Velocity Distribution in Scour Hole Region:

Velocity contours, in cm/sec, are drawn in Fig. (3.15) and Fig. (3.16) for Fr = 0.11 and 0.17 for the case of sand with median size 0.5 mm. The contours gradually rise to the top surface indicating the conversion of velocity head into pressure head. Velocity contours near the scour hole dip down into the scour hole. Details of velocity distribution in the deepest portion and very near to the armoured bed could not be recorded because of the large size of the current meter.

3.8 Static Pressure Distribution in the Scour Hole:

Pressure coefficient contours have been plotted in Figs. (3.15, 3.16 and 3.17). Static pressure on the line of symmetry gradually recovers as the flow approaches the cylinder. The contours dive down into scour hole indicating the sinking of vortex in the scour hole.

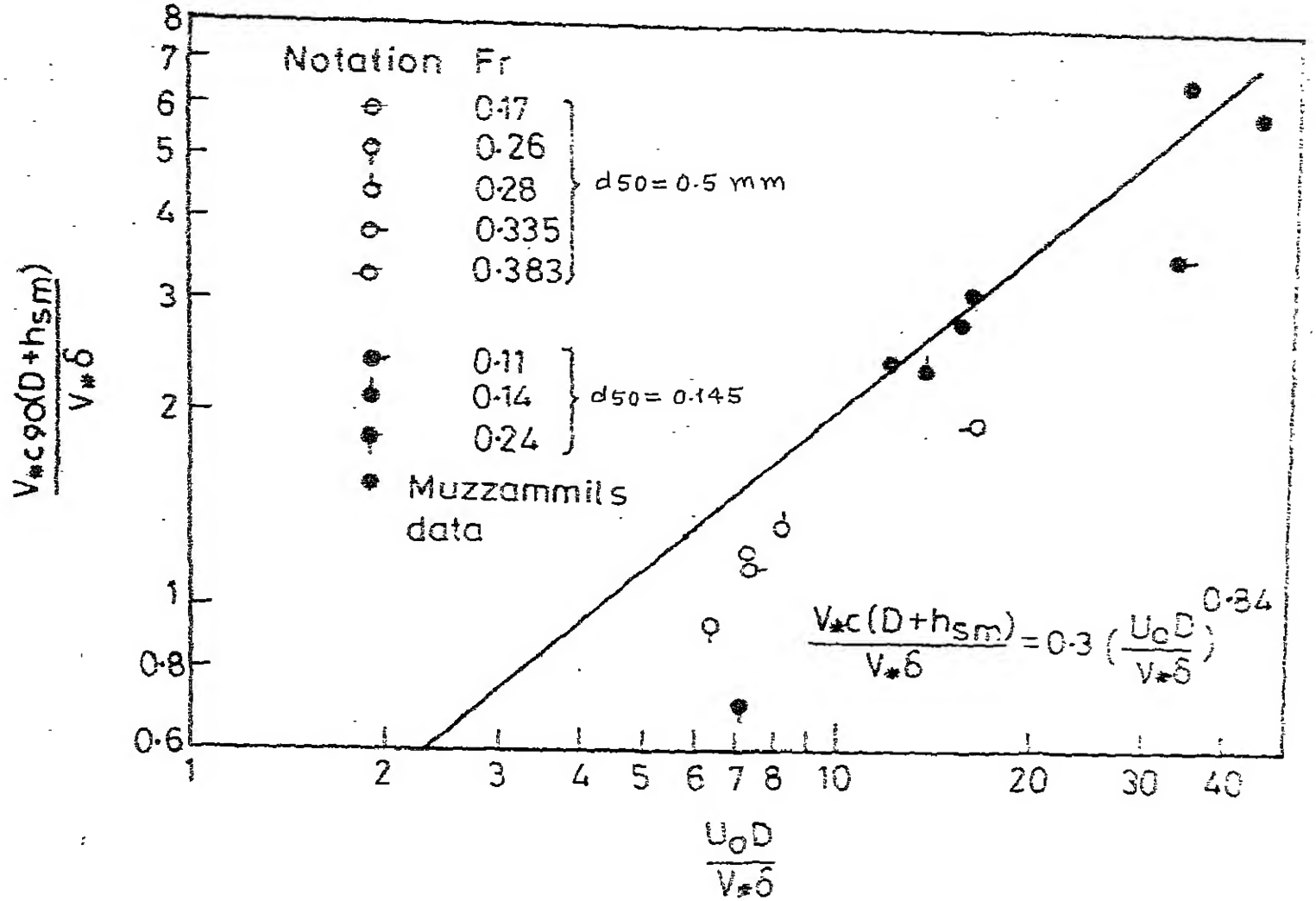

FIG. 3·14 VORTEX STRENGTH RELATIONSHIPS

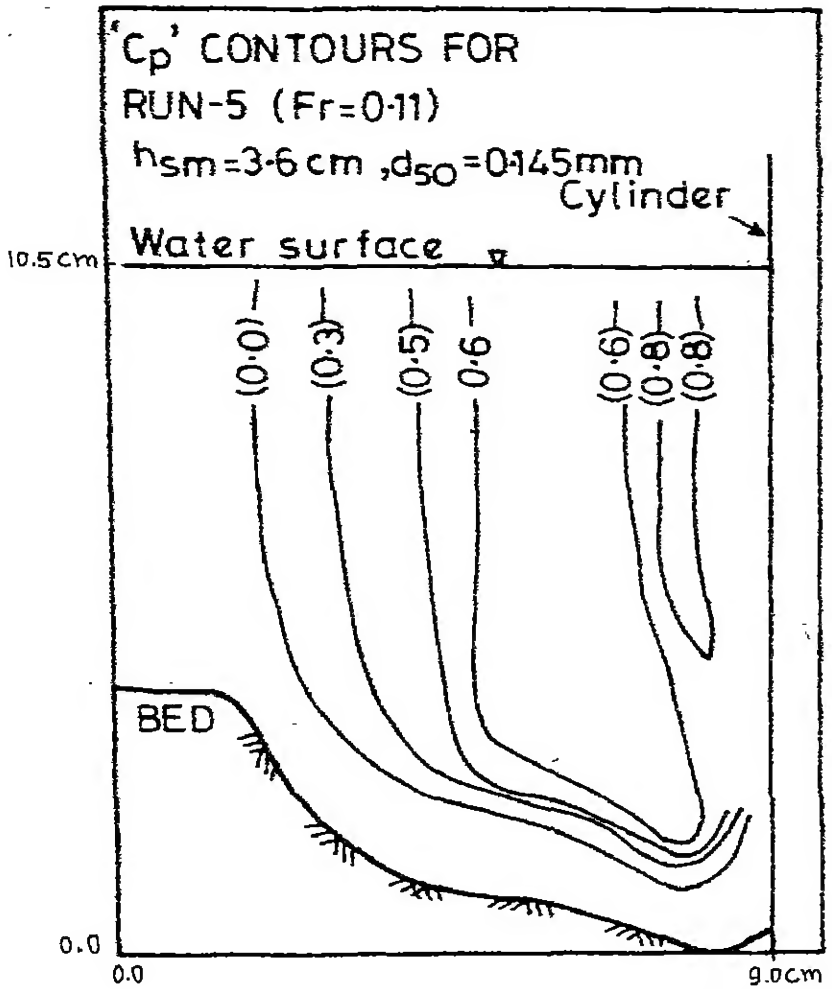

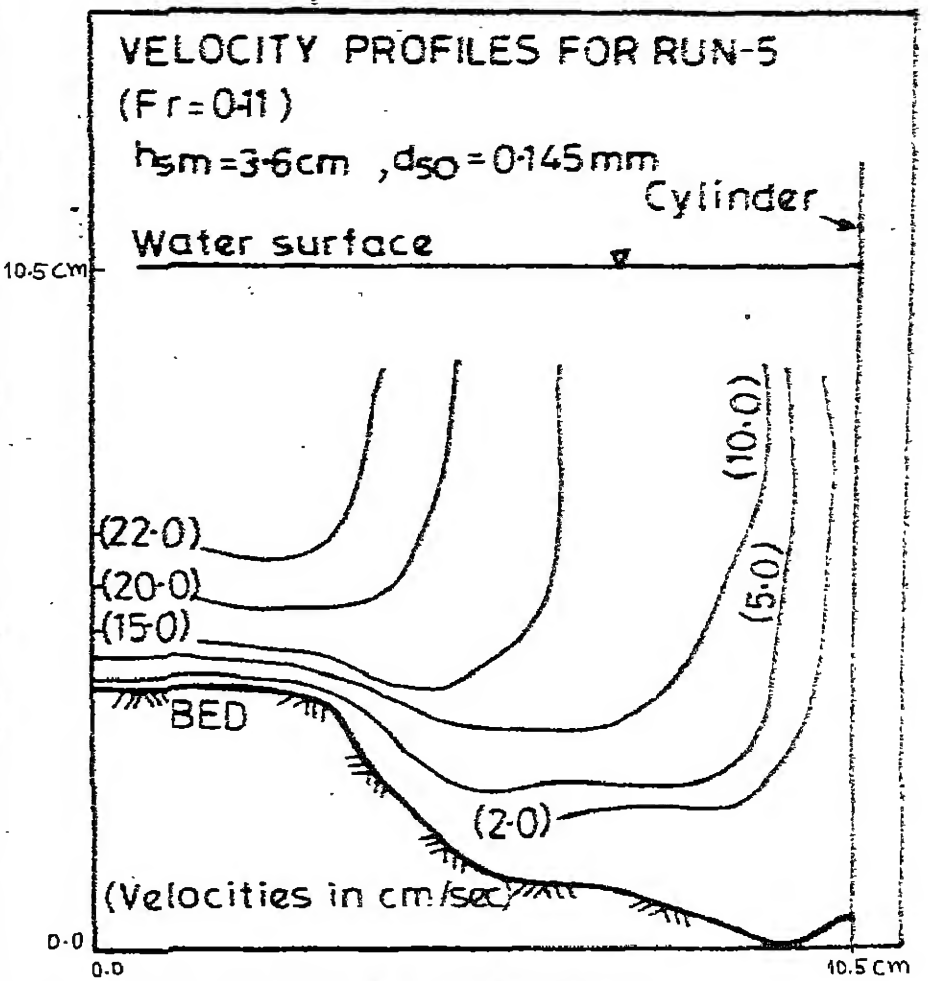

FIG·3·15 PRESSURE AND VELOCITY CONTOURS

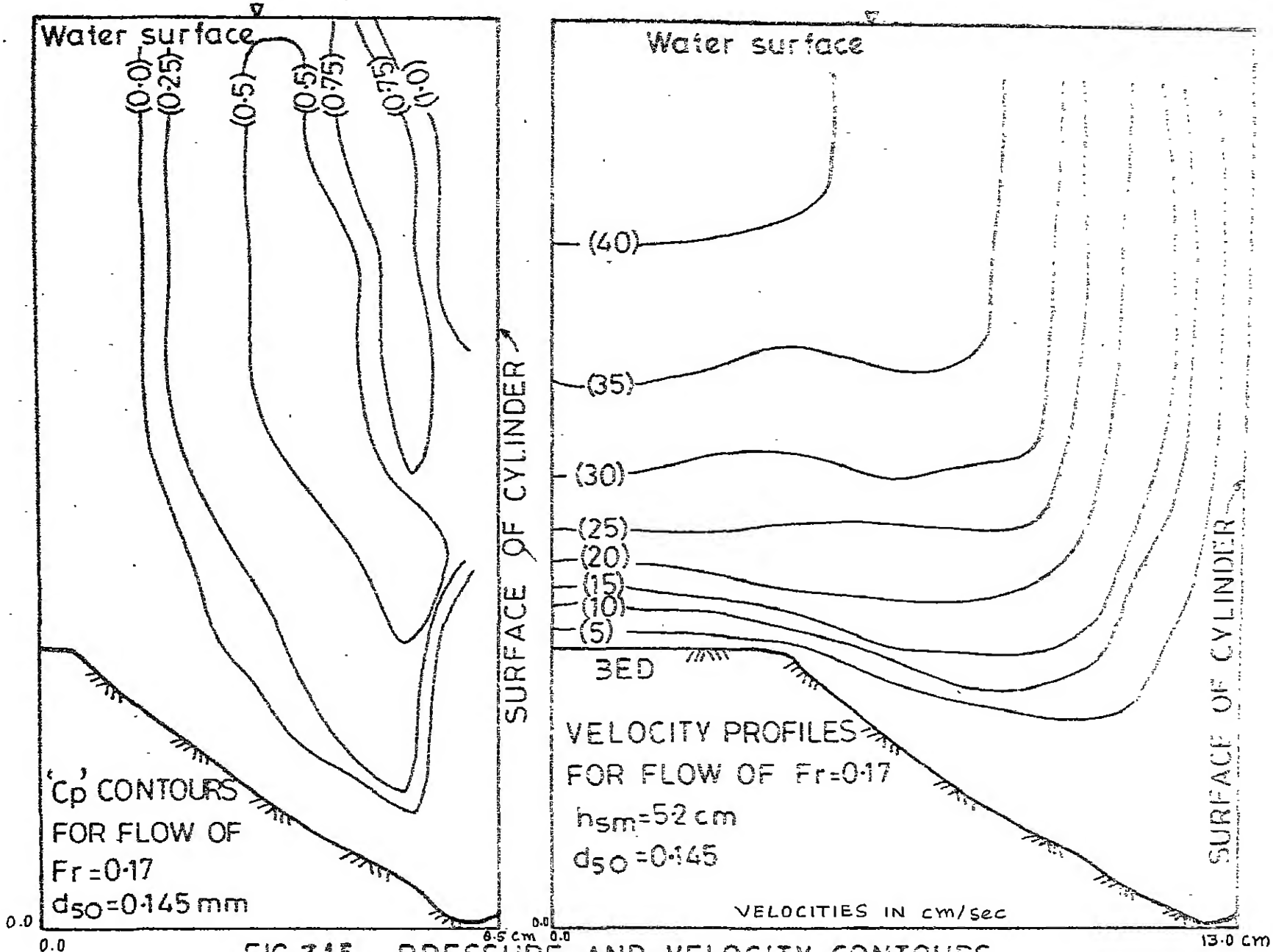

FIG. 3·16 PRESSURE AND VELOCITY CONTOURS

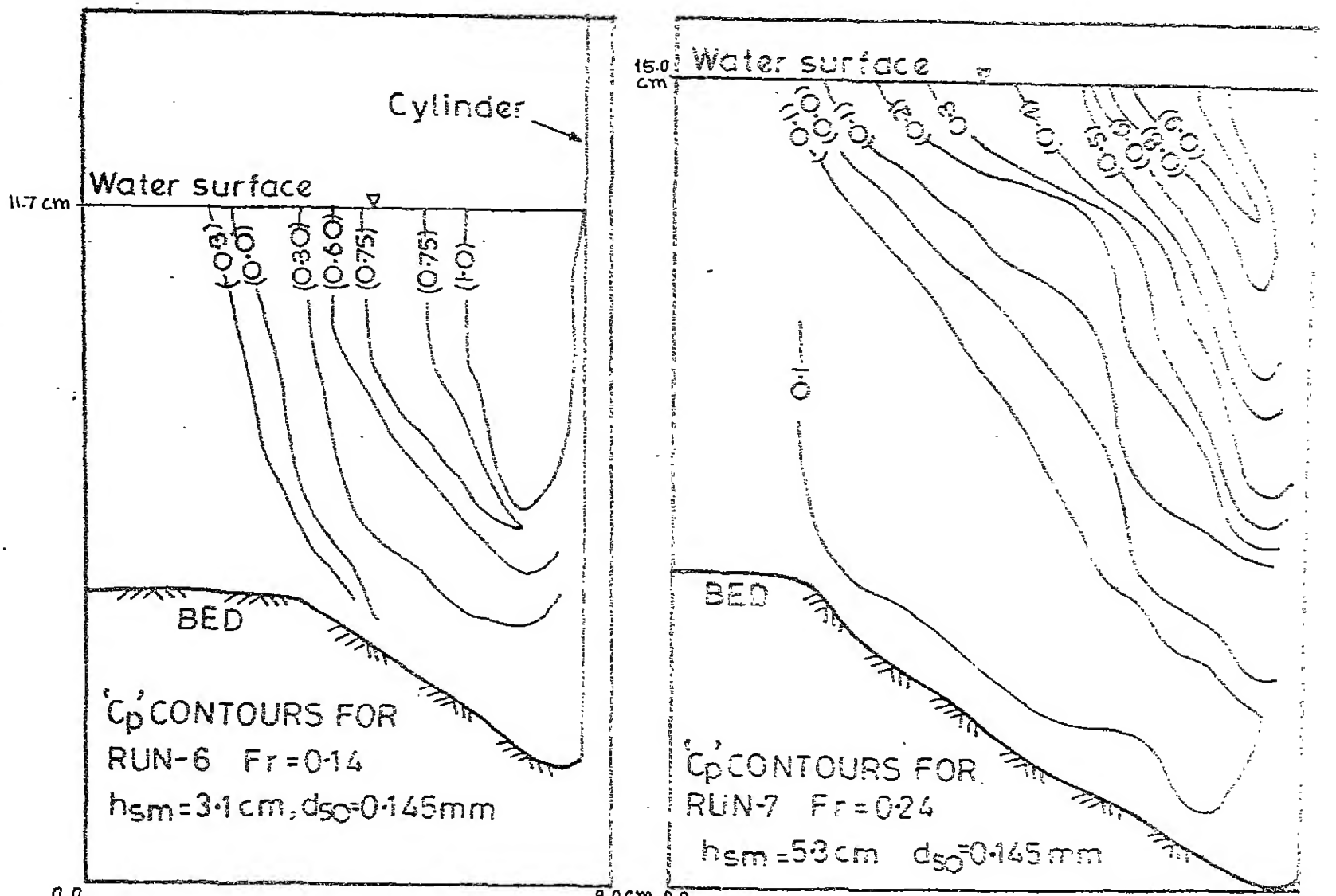

FIG. 3.7 PRESSURE CONTOURS

CHAPTER 4

CONCLUSIONS AND RECOMMENDATIONS

4.1 Conclusions

The following conclusions may be drawn from the present work.

(a) Combining various inferences from the analysis of Melville and Raudkivi's (8) data one may conclude that vortex in the scour hole is of elliptical shape and forced vortex type, having its minor axis scale unaltered and major axis scale increasing with increase in scour depth. Vorticity along the different elliptical paths for a particular position of the vortex remains fairly constant, but it decays very fast with increase in scour depth.

(b) Analysis of the data of Baker (2), Gupta (5), Muzzammil (9) and Qadar (11) shows that the initial vortex strength decreases with pier Reynolds number. The size of the vortex decreases gradually with increase in pier Reynolds number and remains fairly constant ($\frac{2r}{D} = 0.2$) at higher pier Reynolds numbers.

(c) From the present experimental study, vorticity is found to be directly related to rate of scour hole development, which decreases with increase in scour depth. Vorticity at equilibrium scour condition is a function of maximum

scour depth and threshold velocity of the armour coat. A model for scour depth prediction is developed based on the relationship of initial vorticity to equilibrium vorticity, in terms of Pier Reynolds number.

(d) Contours of velocity and pressure distribution in a region near the scour hole have been studied. Static pressure is found to recover as the flow approaches the cylinder in the scour hole region and also along the depth of the cylinder. Velocity contours are inclined into the scour hole indicating the sinking of the vortex in the scour hole.

4.2 Recommendations:

In the present work vorticity was measured with the help of a probe which gave vorticity values 0.1 times those obtained from the data of Qadar, Muzzammil, Gupta and Baker for corresponding pier Reynolds number. This has to be investigated. One probable cause may be friction at the bearings. Use of better bearings or some still better device may eliminate this difference.

REFERENCES

1. Baker,C.J. (1979), Laminar Horse-shoe Vortex. Journal of Fluid Mechanics, Vol.95, Part 2, pp. 347-367.

2. Baker, C.J. (1980), Theoretical Approach to Prediction of Local Scour Around Bridge Piers. Journal of Hydraulic Research. Vol.18, No.1, pp. 1-12.

3. Baker, C.J. (1984), The Position of Points of Maximum and Minimum Shear Stress Upstream of Cylinders Mounted Normal to Flat Plates. Journal of Wind Engineering and Industrial Aerodynamics, 18(1985) 263-274.

4. Breusers, H.N.C., G. Nicollet, and H.W. Shen, (1977), Local Scour Around Cylindrical Piers, Journal of Hydraulic Research, Vol.15, No. 3, pp. 211-252.

5. Gupta, A.K. (1984): 'Experimental Investigation: Boundary Layer Flow Past a Circular Cylinder Mounted on a Flat Plate', M.Tech. Thesis, Department of Civil Engineering, Indian Institute of Technology,Kanpur.

6. Laursen, E.M. and Toch, A. (1956), Scour Around Bridge Piers and Abutments, Proc. IAHR, Int. Hydr. Conf. Minnesota, pp. 123-131.

7. Melville, B.W. (1975): 'Local Scour at Bridge Sites', Univ. of Auckland, School of Engg. Auckland, Newzeeland, Rep. No. 117.

8. Melville, B.W. and Raudkivi,A.J. (1977), Flow Characteristics in Local Scour at Bridge Piers, Journal of Hydraulic.

9. Muzzammil , M. (1985): 'Experimental Investigation: Open Channel Flow Past a Circular Cylinder Mounted on a Rigid Bed and on a Mobile Bed', M.Tech. Thesis, Department of Civil Engineering Indian Institute of of Technology, Kanpur.

10. Posey, C.J. (1974), Tests of Scour Mechanism at Bridge Piers, Proc. ASCE, Vol. 10, HY 12, pp. 1773-1783.

11. Qadar, A. (1981), The Vortex Scour Mechanism at Bridge Piers, Proc. Inst. Civil Engrs. Part 2, Vol.71, pp. 739-757.

12. Roper, A.T., Schneider, V.R. and Shen, H.W. (1967), Analytical Approach to Local Scour, Proc. 12th IAHR, Congress, Fort Collins, 3, pp. 151-161.

13. Gangadharaiah, T., Muzzammil, M. and Subramanya, K., Vortex Strength Approach for Bridge Pier Scour Predictions, Second International Workshop on, Alluvial River Problems, University of Roorkee, October 24-26, 1985.

CE-1986-M-GUP-CHA